

Conformer-specific Chemistry Imaged in Real Space and Time

E. G. Champenois,^{1,†} D. M. Sanchez,^{1,2,†,‡} J. Yang,^{1,3,4} J. P. F. Nunes,⁵ A. Attar,³ M. Centurion,⁵ R. Forbes,³ M. Gühr,⁶ K. Hegazy,¹ F. Ji,³ S. K. Saha,⁵ Y. Liu,⁷ M.-F. Lin,³ D. Luo,³ B. Moore,⁵ X. Shen,³ M. R. Ware,¹ X. J. Wang,^{3,*} T. J. Martínez,^{1,2,*} & T. J. A. Wolf^{1,*}

Affiliations:

¹Stanford PULSE Institute, SLAC National Accelerator Laboratory, Menlo Park, USA.

²Department of Chemistry, Stanford University, Stanford, USA.

³SLAC National Accelerator Laboratory, Menlo Park, USA.

⁴Center of Basic Molecular Science, Department of Chemistry, Tsinghua University, Beijing, China.

⁵Department of Physics and Astronomy, University of Nebraska-Lincoln, Lincoln, USA.

⁶Institut für Physik und Astronomie, Universität Potsdam, Potsdam, Germany.

⁷Department of Physics and Astronomy, Stony Brook University, Stony Brook, NY, USA.

*Corresponding authors. Emails: thomas.wolf@stanford.edu, toddjmartinez@gmail.com, wangxj@slac.stanford.edu

† These authors contributed equally to this work.

Abstract:

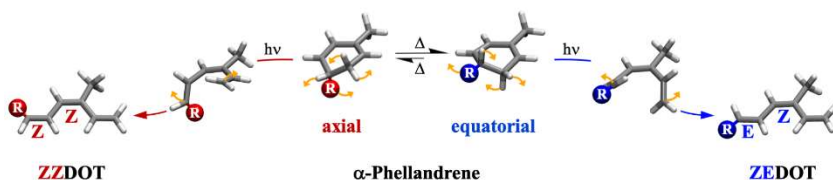
Conformational isomers or conformers of molecules play a decisive role in chemistry and biology. However, experimental methods to investigate chemical reaction dynamics are typically not conformer-sensitive. Here, we report on a gas-phase megaelectronvolt ultrafast electron diffraction investigation of α -phellandrene undergoing an electrocyclic ring-opening reaction. We directly image the evolution of a specific set of α -phellandrene conformers into the product isomer predicted by the Woodward-Hoffmann rules in real space and time. Our experimental results are in quantitative agreement with nonadiabatic quantum molecular dynamics simulations, which provide unprecedented detail of how conformation influences time scale and quantum efficiency of photoinduced ring-opening reactions. Due to the prevalence of large numbers of conformers in organic chemistry, our findings impact our general understanding of reaction dynamics in chemistry and biology.

Main Text:

Conformational isomers, or conformers, can interconvert via rotations around single chemical bonds. Interconversion between conformers represents an important step in many bi-molecular reactions, where reactant species must not only encounter one-another in a particular orientation, but also in a specific structural conformation.⁽¹⁾ Moreover, conformer dynamics arise naturally in self-ordering of macromolecular structures, e.g., protein folding.⁽²⁾ However, investigation of conformer-specific dynamics on their natural time and length scales of femtoseconds and Ångströms is hindered by the insensitivity of established experimental methods to conformers.

The influence of conformers on photochemical reactivity is well-known, e.g. from electrocyclic reactions according to the Woodward-Hoffmann (WH) rules.⁽³⁾ These rules predict them to be concerted and

a) Woodward-Hoffman Predicted Products



b) Photochemistry of α -Phellandrene

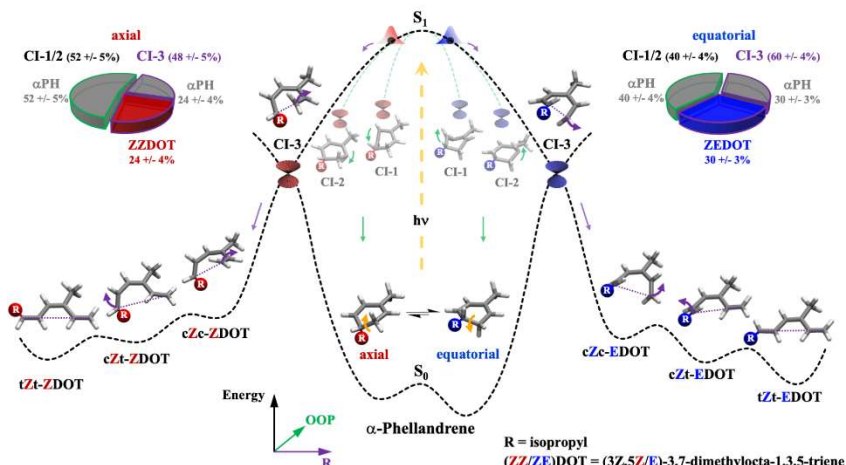


Fig. 1. Conformer-Specific Photochemistry in α -Phellandrene. a) Woodward-Hoffmann predictions for the conformer-specificity of photoinduced electrocyclic ring-opening in α -phellandrene. Its isopropyl substituent (R) can be in axial or equatorial orientation with respect to the carbon ring. Axial and equatorial conformers are in thermal equilibrium in solution phase (Δ).⁽⁶⁾ The Woodward-Hoffmann rules predict a concerted, conrotatory ring-opening motion (orange arrows) yielding isomers with R in different positions depending on the reactant conformer. b) Schematic based on *ab initio* multiple spawning simulations of the photoinduced ring-opening. Equatorial and axial conformers are photoexcited from their respective ground state (S_0) energy minima to the first excited state (S_1), they evolve along an out-of-plane (green, OOP) towards conical intersections (CI) CI-1 and CI-2 or along the ring-opening coordinate (purple) towards CI-3. CI-1/CI-2 lead to reformation of α -Phellandrene while CI-3 leads to both α PH reformation and ring-opening. Several different conformers of the Z/E DOT photoproduct minima (cZc, cZt, and tZt) are accessible in the ground state. The two pie charts visualize the photoproduct distribution for axial and equatorial conformers as well as the distribution among the CI geometries CI-1 to CI-3 with errors representing 68% confidence intervals obtained from bootstrap analysis.

a concerted, conrotatory motion i.e., both ends of the newly formed open-ring molecule rotate away from each other in the same clockwise or counterclockwise direction (see **Fig. 1a**). This motion leads to different photoproducts depending on the reactant conformer, the isomers (3Z,5E)-3,7-dimethylocta-1,3,5-triene (ZEDOT, from eq- α PH) and (3Z,5Z)-dimethylocta-1,3,5-triene (ZZDOT, from ax- α PH, see **Fig. 1**).

Evidence for the conformer-specificity of the ring-opening in α PH⁽⁶⁾ and other reactants^(8, 9) has been observed in solution-phase measurements of photoproduct ratios. Moreover, resonance Raman

conformer-specific, i.e., leading to different reaction products depending on the reactant conformer. Electrocyclic reactions play an important role e.g., in chemical synthesis⁽⁴⁾ and the Vitamin D production in human skin.⁽⁵⁾

An instructive example for conformer-specificity is the photochemical ring-opening of the monoterpene α -phellandrene (α PH),⁽⁶⁾ which is produced by plants and used in the fragrance, food, and pharmaceutical industries.⁽⁷⁾ α -Phellandrene consists of a 1,3-cyclohexadiene (CHD)-like ring moiety with two substituents, an isopropyl group at its sp^3 hybridized C_1 position and a methyl group at the C_8 position (see **Figs. 1** and **2**). The substitution gives rise to two conformers with the isopropyl group being in either quasi-axial (ax) or -equatorial (eq) orientation, (i.e., approximately perpendicular or parallel to the ring plane, respectively). The WH rules predict the ring-opening to take place in

investigations revealed evidence for the significance of conrotatory motion in the depopulation of the Franck-Condon region of the reactant excited state.(10) The photochemical dynamics leading from the Franck-Condon region to the ring-opened photoproducts of α PH have been investigated by several ultrafast spectroscopic studies in both the gas and condensed phase, however largely without sensitivity to the structural dynamics, reactant conformers, or photoproduct isomers.(11-15)

Here, we report on a combined megaelectronvolt ultrafast electron diffraction (UED) and *ab initio* multiple

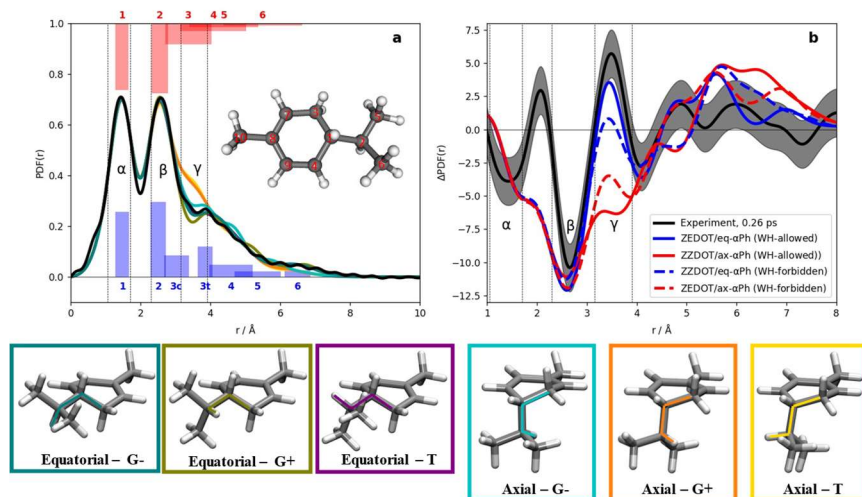


Fig. 2. Comparison of experimental and simulated structural information. a) Experimental (black) and simulated pair distribution functions PDF(r) of six α -phellandrene conformers, which are depicted below together with the dihedral angles defining the rotation of the isopropyl group. Carbon-Carbon coordination spheres for axial (red) and equatorial (blue) conformers are shown as bars. Additionally, the α , β , and γ ranges of **Fig. 3** are shown. The inset shows the Carbon atom numbering used in the text. b) Experimental difference PDF at a pump-probe delay of 0.26 ps (black) and simple simulations of the signature of Woodward-Hoffmann-(WH)-allowed and WH-forbidden reaction product signatures. Error bars represent a 68% confidence interval obtained from bootstrap analysis.

spawning (AIMS)(16-18) study of conformer-specific dynamics in the photochemical ring-opening of gas-phase α PH with unambiguous conformer-sensitivity confirming but going far beyond the qualitative orbital-symmetry based WH rule predictions. In both our static diffraction measurements and quantum chemical calculations, we find the eq- α PH conformer to dominate in our gas phase sample (see **supplementary note 1**). As opposed to all other studies of electrocyclic reactions, our time-resolved measurements directly image concerted and exclusive formation of the ZEDOT photoproduct predicted by the WH rules on the femtosecond timescale with

sub-Å resolution and in quantitative agreement with AIMS simulations of the photochemical dynamics.

The simulations reveal that after photoexcitation into the lowest excited state (S_1) with $\pi\pi^*$ character, α PH non-adiabatically relaxes to the electronic ground state (S_0) through three different conical intersection (CI) geometries.(19) Only one of them yields ring-opened photoproducts while the other two form vibrationally “hot” reactant. The presence of the isopropyl group redirects significant amounts of the S_1 population towards the non-WH CIs, substantially reducing the WH-photoproduct yield compared to CHD.(20) Additionally, the rotational orientation of the isopropyl group gives rise to three rotational conformers (rotamers) for each of the eq and ax- α PH structures, labeled as gauche+/- (G+/G-) and trans (T, see **Fig. 2**), which are simultaneously present in our sample. These rotamers show significantly different ring-opening time scales.

Figure 2a shows the extracted static atomic pair distribution function (PDF(r)) from a gas phase sample of randomly oriented α PH molecules. For comparison, we plot simulated PDFs of all six ax-/eq- α PH rotamer geometries. We analyze the structural information contained in the PDFs in terms of Carbon coordination shells, which are additionally plotted as bars for the eq- α PH (blue) and ax- α PH (red) conformers in **Fig. 2a**:

The many C-C bonds (first Carbon coordination shell, labeled as α) in the system give rise to a strong maximum in all PDFs at 1.4 Å, while a second peak at 2.4 Å corresponds to the second Carbon coordination shell (the distances between Carbon atoms two atomic sites away from each other, β in **Fig. 2a**) with some contributions from the third coordination shell (distances of Carbons three atomic sites apart from each other). The signatures above 3 Å belong to the third and higher coordination shells.

We find the most significant differences between the PDFs within the third coordination shell (γ in **Fig. 2**). All eq- α PH and the ax-G- α PH rotamer as well as the experimental PDF exhibit a minimum around 3.5 Å, in contrast to the two remaining ax- α PH rotamers that produce a shoulder. The minimum results from a splitting of the third coordination shell in the eq- α PH and ax-G- α PH rotamers into distances between Carbons in cis-configuration (small dihedral angles, 3c in **Fig. 2a**) e.g., C₃-C₉, and trans-configuration (large dihedral angles, 3t in **Fig. 2a**) e.g., C₃-C₁₀. The splitting collapses for the ax-G+ and ax-T rotamers due to one of the methyl groups of the isopropyl substituent being directly below the Carbon ring and thereby moving many of the ring-Carbon/methyl-carbon distances into the γ region (see structures in **Fig. 2**). The high level of agreement of the experimental PDF with those of eq- α PH and disagreement with some of the ax- α PH PDFs suggests the sample is dominated by eq- α PH rotamers in agreement with our quantum chemical calculations (see **supplementary note 1**) and previous results.⁽²¹⁾

The structural dynamics information contained in the time-dependent difference PDF (Δ PDF, difference between PDF(t) and steady-state PDF, see **Fig. 2b**) can be qualitatively understood from “simple” Δ PDF simulations generated from single photoproduct and reactant geometries. As shown in **Fig. 1b**, the ZEDOT and ZZDOT photoproducts can visit several ground state minima, which are all energetically accessible due to the high amount of nuclear kinetic energy in the photoproducts.⁽²²⁾ These minima differ by the dihedral angles between the double bonds, i.e., their orientation relative to each other with respect to the connecting single bonds. Each terminal double bond can be either in cis (c) or trans (t) orientation to the central double bond. It is conceivable that ZEDOT will be found more often in cZc-like configurations, since the geometry is closest to the eq- α PH reactant geometry. Moreover, like in the reactant geometry, the bulky isopropyl group is pointing away from the rest of the molecule. In ax- α PH, on the other hand, the conrotatory motion rotates the isopropyl group into the rest of the molecule, making cZc-like geometries significantly more unstable. The prevalence for cZc-ZEDOT (eq- α PH) and tZt-ZZDOT (ax- α PH) geometries is also reflected by our AIMS simulations (see below and **Fig. S1**). Therefore, the qualitative Δ PDF simulations are based on cZc-EDOT and tZt-ZDOT geometries.

Figure 2b shows an experimental Δ PDF 260 fs after photoexcitation with an ultrashort 266 nm optical pulse. We compare it with photoproduct Δ PDF simulations of the WH-predicted photoproducts eq- α PH \rightarrow cZc-EDOT (blue line) and ax- α PH \rightarrow tZt-ZDOT (red line). Additionally, we depict the WH-forbidden reactant/product Δ PDFs eq- α PH \rightarrow tZt-ZDOT (blue dots) ax- α PH \rightarrow cZc-EDOT (red dots). Atomic distance changes appear in Δ PDFs as a combination of a negative contribution at the initial atomic distance and a positive contribution at the delay-dependent distance. Accordingly, all Δ PDFs in **Fig. 2b** show signatures from ring-opening: The negative signature in the α -region directly follows from breaking the C₁-C₃ bond, while the negative signature in the β -region mainly results from increases in the C₁-C₇, C₂-C₃, and C₃-C₄ distances. Like the static PDFs, experimental and simulated Δ PDFs show the most prominent differences in the γ -region. Differences between experimental and simulated Δ PDFs in the α and β regions are due to the approximation of the photoproduct by a single geometry. The WH-allowed photoproduct of the eq-conformers shows good qualitative agreement with a strong positive signature in the γ -region of the experimental Δ PDF, whereas all other Δ PDFs show essentially zero or negative amplitude.

The difference between the simulated Δ PDFs can be explained in the same way as for the steady-state PDFs: The helical structure of the cZc-EDOT photoproduct results in a collapse of the distance splitting in the third coordination shell of the eq- α PH reactant leading to a positive Δ PDF signature in the γ region. In contrast, for the ax- α PH/tZt-ZDOT reactant/photoproduct combination, a splitting of the third coordination shell is induced by the more stretched photoproduct geometry leading to a negative Δ PDF signature. Both effects, the positive signature of eq- α PH/cZc-EDOT and the negative signature of ax- α PH/tZt-ZDOT, are direct results of the orientation of the isopropyl group in the reactant conformer and therefore an unambiguous signature of conformer-specific ring-opening.

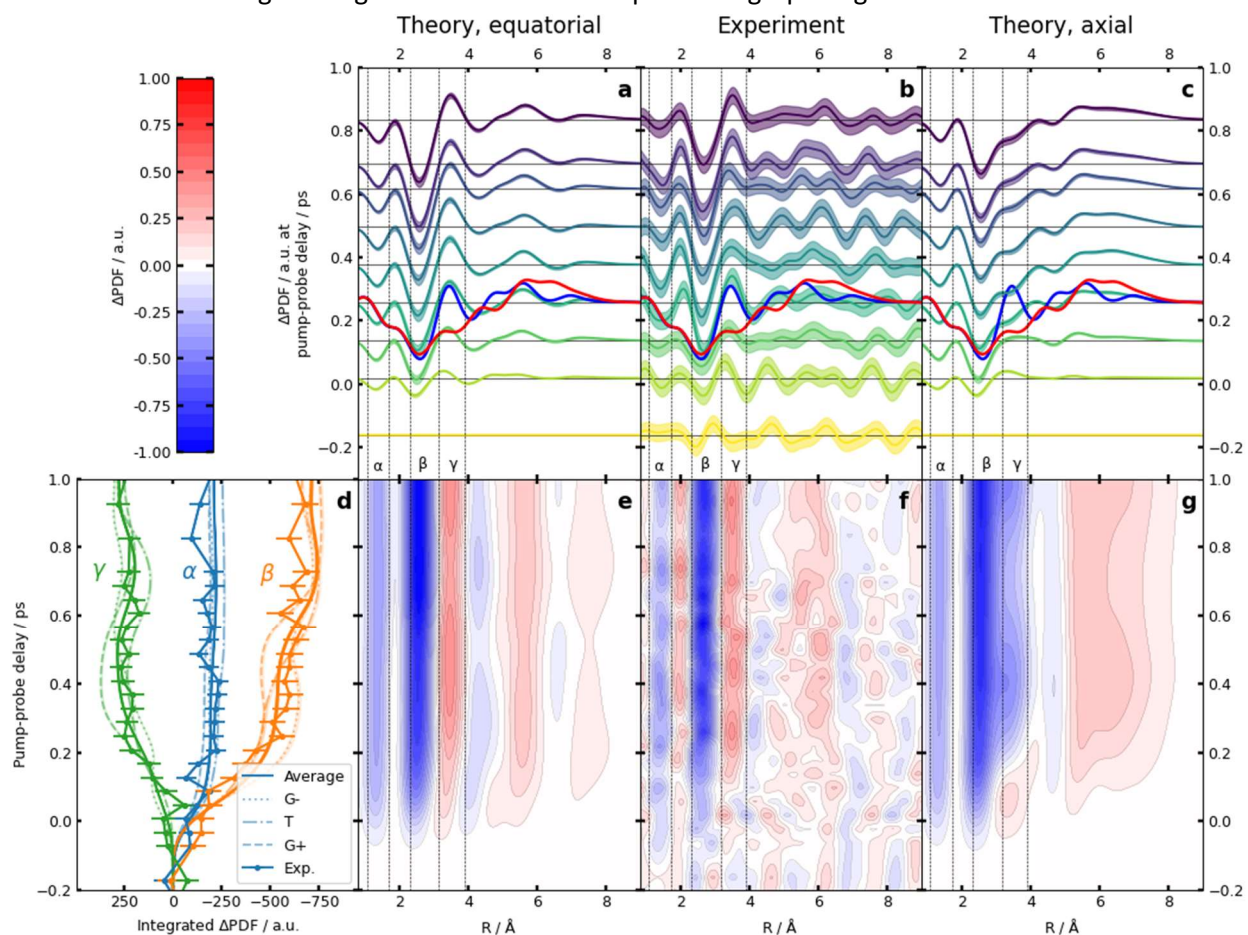


Figure 3: Comparison of experimental (b,f) and simulated time-dependent difference pair distribution functions (Δ PDF) of equatorial (a,d,e) and axial (c,g) conformers. a,b,c) Δ PDFs at different pump-probe delays and e,f,g) false-color plots of Δ PDF over the whole investigated time window. Simulated Δ PDFs are based on ab-initio multiple spawning simulations (see methods). Δ PDFs at a delay of 260 fs in a,b,c are superimposed with the simulations of the conformer-specific Woodward-Hoffmann-allowed photoproducts for the axial (red) and equatorial (blue) conformers from Fig. 2b. d) Comparison of integrated signals in the α , β , and γ regions from the experiment, the averaged and the individual eq-rotamer simulations. Error bars represent a 68 % confidence interval obtained from bootstrap analysis. For the simulations, these error bars reflect convergence with respect to initial condition sampling.

The experimental Δ PDFs (Fig. 3b and f) are compared with those computed from AIMS simulations(18) (Fig. 3a, c, e, and g) using α -state-averaged complete active-space self-consistent field theory (α -CASSCF)(23) and assuming roughly equal contributions from the individual G-, T, and G+ rotamers at room temperature. The averaged AIMS Δ PDFs of the eq-conformers show quantitative agreement with the

experimental data within their signal-to-noise level while the averaged AIMS Δ PDFs of the ax-conformers qualitatively disagree with the experimental data in the γ region. The experimental time-dependent signatures are clearly dominated by the eq- α PH rotamers (>80%, see **supplementary note 1**). Thus, we unambiguously observe exclusive formation of the WH-predicted photoproducts of the eq- α PH conformer within a few hundred fs after optical excitation. Our results constitute the first direct observation of conformer-specific chemical reaction dynamics in real space and time.

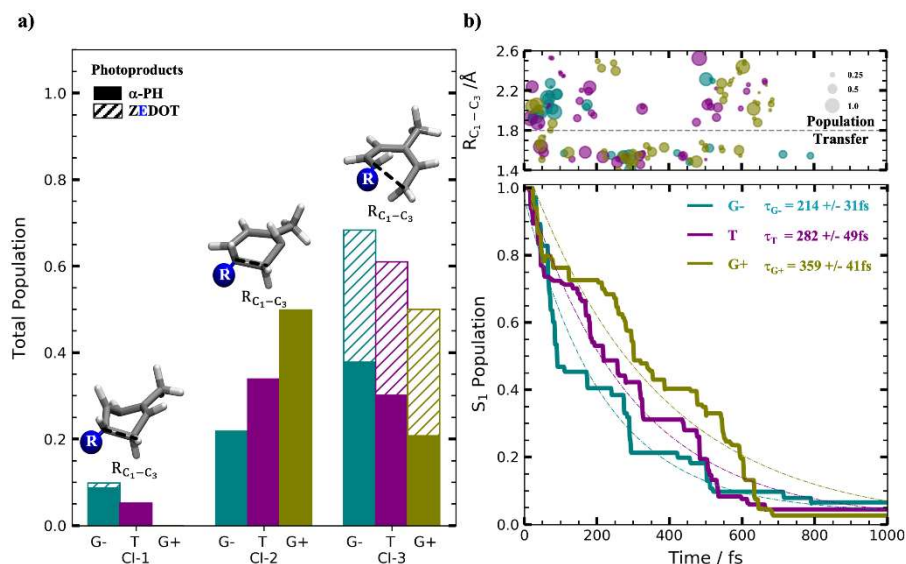


Figure 4. Characterization of the Closed- and Open-Ring Nonradiative Relaxation Pathways of eq-Rotamers. a) Histogram of the branching ratio between the closed and open pathways from simulations. Solid and striped bars represent fractional population that reform α PH or ZEDOT, respectively. b) (top) The C_1 - C_3 distance vs population transfer time from S_1 to S_0 for all 45 eq initial conditions (see methods). The black dashed line corresponds to the threshold used to determine if the ring is open or closed. The circle radius is proportional to the amount of population involved in the transfer event and separated into the three rotamers. (bottom) The S_1 population decay for the three eq-rotamers in the first ps after photoexcitation.

observe a hitherto unknown secondary ring-closure reaction in the electronic ground state yielding 2-ladderane (5-isopropyl-2-methylbicyclo[2.2.0]hex-2-ene). The ring-closure is exclusively observed for the fraction of population undergoing internal conversion through CI-1 in the ground state (see **supplementary note 2**). Non-WH relaxation pathways have been observed before for the prototypical CHD molecule(22), but had marginal contributions to the relaxation process. The presence of the isopropyl substituent redirects 40 ± 4 % of the eq- α PH S_1 population towards non-WH pathways and, thus, substantially reduces the ring-opening quantum yield (see **Fig. 1b**).

The time dependence of the measured and computed Δ PDFs in the α , β , and γ regions are shown in **Figs. 3d** and **S3b** for the eq and ax conformers, respectively. The averaged simulation assuming equal distribution of the three eq-rotamers (G-, T, and G+) leads to quantitative agreement with experiment, whereas individual eq-rotamer contributions to the Δ PDFs are quite distinct (see **Fig. 3d**). Thus, the rotational orientation of the isopropyl group must influence mechanism and time scale of ring-opening. This becomes obvious in **Fig. 4b**, top, where simulated non-adiabatic population transfer events are

Our AIMS simulations reveal additional aspects of the relaxation process, which cannot be easily extracted from the experimental data. α -Phellandrene relaxes via the WH-predicted conrotatory ring-opening motion through a CI (CI-3) yielding both ring-opened photoproducts and the closed-ring reactant (see **Figs. 1b, 4a**, and **S2**). Due to its differential nature, the Δ PDF observable is preferentially sensitive to the part of the population undergoing ring-opening. Additionally, out-of-plane bending in S_1 leads through two CIs (CI-1/CI-2) to the closed-ring reactant (**Table S1**). Furthermore, we

categorized with respect to their C₁-C₃ distances at the time of the transfer event i.e., their ability to undergo ring-opening and, thus, to significantly contribute to the Δ PDF observable (see above). In the case of the eq-G- rotamer, almost all population undergoing ring-opening relaxes to S₀ within 200 fs after photoexcitation. The other two rotamers show substantially less ring-opening in this timeframe. Their remaining population undergoes ring-opening significantly later, 500-700 fs after photoexcitation. The difference in ring-opening timescale is clearly reflected in the time-dependent Δ PDF amplitudes in **Fig. 3d**.

In summary, in the combination of UED with AIMS simulations, we directly observe conformer-specific reaction dynamics on their natural time and length scales in agreement with the Woodward-Hoffmann rules. Moreover, we observe considerable effects on the efficiency and timescale of the reaction from the presence and orientation of an isopropyl substituent of the molecule. Similar conformer-dependent photochemistry has been observed only in a limited number of studies of photoproduct distributions, mostly after conformer-specific resonance-enhanced photoionization.^(1, 24-26) Our study marks to the best of our knowledge, the first time-domain observation of such conformer-specific photochemical dynamics. We speculate that the paucity of previous observations of conformer and rotamer-specificity is due to the absence of suitable experimental observables. These findings could have a large impact on our understanding of photochemical reaction mechanisms, since organic structures are prone to a large number of ground state conformers and rotamers. Future investigations of photochemical dynamics using single molecule methods with structural sensitivity, e.g. Coulomb explosion imaging at free electron lasers, might prove strongly conformer-specific photochemistry to be rather the rule than the exception.

Acknowledgments:

We thank J. P. Cryan, M. C. Hoffmann, R. K. Li, M. Niebuhr, S. Weathersby, and T. Weinacht for their help and fruitful discussions. Lawrence Livermore National Laboratory is operated by Lawrence Livermore National Security, LLC, for the U.S. Department of Energy, National Nuclear Security Administration under Contract DE-AC52-07NA27344.

This work was supported by the AMOS program within the US Department of Energy, Office of Science, Basic Energy Sciences, Chemical Sciences, Geosciences, and Biosciences Division.

The experimental part of this research was performed at the SLAC MeV UED facility, which is supported in part by the DOE BES SUF Division Accelerator & Detector R&D program, the Linac Coherent Light Source (LCLS) Facility, and SLAC under contract nos. DE-AC02-05-CH11231 and DE-AC02-76SF00515.

M.G. is funded via a Lichtenberg Professorship of the Volkswagen Foundation.

D.M.S. is grateful to the NSF for a graduate fellowship.

M.C. is supported by the US Department of Energy Office of Science, Basic Energy Sciences under award no. DE-SC0014170.

Y.L. is supported by the US Department of Energy Office of Science, Basic Energy Sciences under award no. DE-FG02-08ER15984

References:

1. Y.-P. Chang *et al.*, Specific Chemical Reactivities of Spatially Separated 3-Aminophenol Conformers with Cold Ca⁺ Ions. *Science* **342**, 98 (2013).
2. K. A. Dill, J. L. MacCallum, The Protein-Folding Problem, 50 Years On. *Science* **338**, 1042-1046 (2012).
3. R. B. Woodward, R. Hoffmann, The Conservation of Orbital Symmetry. *Angew. Chem. Int. Ed* **8**, 781-853 (1969).

4. T. Bach, J. P. Hehn, Photochemical Reactions as Key Steps in Natural Product Synthesis. *Angew. Chem. Int. Ed.* **50**, 1000-1045 (2011).
5. E. Havinga, J. L. M. A. Schlatmann, Remarks on the specificities of the photochemical and thermal transformations in the vitamin D field. *Tetrahedron* **16**, 146-152 (1961).
6. J. E. Baldwin, S. M. Krueger, Stereoselective photochemical electrocyclic valence isomerizations of α -phellandrene conformational isomers. *J. Am. Chem. Soc.* **91**, 6444-6447 (1969).
7. M. M. de Christo Scherer *et al.*, Wound healing activity of terpinolene and α -phellandrene by attenuating inflammation and oxidative stress in vitro. *J. Tissue Viability* **28**, 94-99 (2019).
8. W. G. Dauben, J. Rabinowitz, N. D. Vietmeyer, P. H. Wendschuh, Photoequilibria between 1,3-cyclohexadienes and 1,3,5-hexatrienes. Photochemistry of 3-alkyl-6,6,9,9-tetramethyl- $\Delta^{3,5(10)}$ -hexalins. *J. Am. Chem. Soc.* **94**, 4285-4292 (1972).
9. C. W. Spangler, R. P. Hennis, The influence of ground state conformation on the photochemical ring-opening of 5-alkylcyclohexa-1,3-dienes. *Chem. Commun.*, 24-25 (1972).
10. M. K. Lawless, S. D. Wickham, R. A. Mathies, Resonance Raman View of Pericyclic Photochemical Ring-Opening Reactions: Beyond the Woodward-Hoffmann Rules. *Acc. Chem. Res.* **28**, 493-502 (1995).
11. P. J. Reid, S. J. Doig, R. A. Mathies, Picosecond time-resolved UV resonance Raman spectroscopy of the photochemical ring opening of 1,3,5-cyclooctatriene and α -phellandrene. *J. Phys. Chem.* **94**, 8396-8399 (1990).
12. M. Garavelli *et al.*, Reaction Path of a sub-200 fs Photochemical Electrocyclic Reaction. *J. Phys. Chem. A* **105**, 4458-4469 (2001).
13. B. C. Arruda, B. Smith, K. G. Spears, R. J. Sension, Ultrafast ring-opening reactions: a comparison of α -terpinene, α -phellandrene, and 7-dehydrocholesterol with 1,3-cyclohexadiene. *Faraday Discuss.* **163**, 159-171 (2013).
14. O. Njoya, S. Matsika, T. Weinacht, Angle-Resolved Strong-Field Ionization of Polyatomic Molecules: More than the Orbitals Matters. *ChemPhysChem* **14**, 1451-1455 (2013).
15. B. C. Arruda, R. J. Sension, Ultrafast polyene dynamics: the ring opening of 1,3-cyclohexadiene derivatives. *Physical Chemistry Chemical Physics* **16**, 4439-4455 (2014).
16. M. Ben-Nun, T. J. Martínez, Ab initio quantum molecular dynamics. *Adv. Chem. Phys.* **121**, 439-512 (2002).
17. M. Ben-Nun, T. J. Martínez, Nonadiabatic molecular dynamics: Validation of the multiple spawning method for a multidimensional problem. *J. Chem. Phys.* **108**, 7244-7257 (1998).
18. M. Ben-Nun, J. Quenneville, T. J. Martínez, Ab Initio Multiple Spawning: Photochemistry from First Principles Quantum Molecular Dynamics. *J. Phys. Chem. A* **104**, 5161-5175 (2000).
19. S. Matsika, P. Krause, Nonadiabatic Events and Conical Intersections. *Ann. Rev. Phys. Chem.* **62**, 621-643 (2011).
20. A. Hofmann, R. de Vivie-Riedle, Adiabatic approach for ultrafast quantum dynamics mediated by simultaneously active conical intersections. *Chem. Phys. Lett.* **346**, 299-304 (2001).
21. K. M. Marzec, I. Reva, R. Fausto, L. M. Proniewicz, Comparative Matrix Isolation Infrared Spectroscopy Study of 1,3- and 1,4-Diene Monoterpenes (α -Phellandrene and γ -Terpinene). *J. Phys. Chem. A* **115**, 4342-4353 (2011).
22. T. J. A. Wolf *et al.*, The photochemical ring-opening of 1,3-cyclohexadiene imaged by ultrafast electron diffraction. *Nat. Chem.* **11**, 504-509 (2019).
23. J. W. Snyder, R. M. Parrish, T. J. Martínez, α -CASSCF: An Efficient, Empirical Correction for SA-CASSCF To Closely Approximate MS-CASPT2 Potential Energy Surfaces. *J. Phys. Chem. Lett.* **8**, 2432-2437 (2017).
24. M. H. Kim, L. Shen, H. Tao, T. J. Martinez, A. G. Suits, Conformationally Controlled Chemistry: Excited-State Dynamics Dictate Ground-State Reaction. *Science* **315**, 1561 (2007).

25. S. T. Park, S. K. Kim, M. S. Kim, Observation of conformation-specific pathways in the photodissociation of 1-iodopropane ions. *Nature* **415**, 306-308 (2002).
26. K.-W. Choi, D.-S. Ahn, J.-H. Lee, S. K. Kim, A highly conformationally specific α - and β -Ala⁺ decarboxylation pathway. *Chem. Commun.*, 1041-1043 (2007).

Supplementary Information

Conformer-specific Chemistry Imaged in Real Space and Time

E. G. Champenois,^{1,†} D. M. Sanchez,^{1,2,†,‡} J. Yang,^{1,3,4} J. P. F. Nunes,⁵ A. Attar,³ M. Centurion,⁵ R. Forbes,³ M. Gühr,⁶ K. Hegazy,¹ F. Ji,³ S. K. Saha,⁵ Y. Liu,⁷ M.-F. Lin,³ D. Luo,³ B. Moore,⁵ X. Shen,³ M. R. Ware,¹ X. J. Wang,^{3,*} T. J. Martínez,^{1,2,*} & T. J. A. Wolf^{1,*}

Methods

Ultrafast electron diffraction experiments:

The experimental apparatus is described in detail elsewhere.(27) In short, we use the 800 nm output of a Ti:Sapphire laser system and separate two beam paths. Pulses in both beam paths are frequency-tripled. The pulses of the probe beam path are directed onto the photocathode of an RF gun and eject an ultrashort pulse containing $\sim 10^4$ electrons. 3.7 MeV electrons are generated using a S-band photocathode radio frequency (RF) gun(28) and focused through a holey mirror to a spot size of 200 μm FWHM in the interaction region of a gas phase experimental chamber. The pump pulses (7 μJ) are focused into the experimental chamber to a diameter of 240 μm FWHM and overlapped with the electron pulses at a 2° angle. The experimental response function including effects of the optical and electron pulse length as well as relative arrival time jitter is estimated to be 150 fs.(22) αPH is purchased from Sigma-Aldrich and used without further purification. We use a static-filled 3 mm flow cell (550 μm orifices, sample at room temperature) in combination with a repetition rate of 360 Hz. Diffracted electrons are detected by a combination of a phosphor screen and an EMCCD camera. Based on the relative static and dynamic signal levels, we estimate to excite about 2.5 % of the molecules (see **Fig. S4**). Time-dependent diffraction is measured at a series of time delay points between -2 ps and +1 ps in each scan. The separation between time delay points is 50 fs, except for the earliest and latest delay points, where it was considerably larger. At each time delay point, we integrate diffraction signal for 10 seconds. The full data set includes 88 such scans. The sequence of delay steps is randomized for every scan to avoid systematic errors.

Generation of modified molecular diffraction and pair distribution functions from experimental data:

Determination of modified molecular diffraction ($sM(s)$, see **Fig. S5**) from 2-dimensional molecular diffraction data is described in detail in the supplementary information of Ref. (22). Similar to Ref. (22), generation of static atomic pair distribution functions (PDFs, see **Fig. 2a**) requires extrapolating the experimental $sM(s)$ for $s \leq 0.8 \text{ \AA}^{-1}$ with simulated $sM(s)$ signal (see **Fig. S5**). As evident from **Fig. S5**, the extrapolated range (dashed black line) does not show conformer-dependence in the simulations. Thus, our mode of extrapolation does not bias the shape of the PDF towards a specific conformer.

$\Delta sM(s, t)$ is generated by subtracting $sM(s)$ before time zero (before the onset of transient features) from $sM(s)$ of all pump-probe delays. As for PDFs, extrapolation of these traces to $s=0 \text{ \AA}^{-1}$ is required to avoid artifacts in $\Delta\text{PDF}(r, t)$. In this low s region, the traces are set to $\Delta sM_{\text{hole}}(s, t) = \Delta sM_{\text{eq}}(s, t=1\text{ps}) \times (1 + \text{erf}[(t-t_0)/\tau])$. The first term is the average of the simulated $\Delta sM(s, t)$ traces for the three equatorial conformers at a delay of 1 ps. The second term sets the time-dependence, which is assumed to follow a simple error function with the onset time t_0 and width τ found by curve-fitting to $\Delta sM_{\text{eq}}(s, t)$. As described in detail in the supplementary material of Ref.(22), for the generation of $\Delta\text{PDF}(r, t)$, the high s contributions of

$\Delta s_{\text{Meq}}(s,t)$ are smoothly damped using a Gaussian function e^{-ks^2} with $k=0.028 \text{ \AA}^2$. To ensure that the low s extrapolation of the experimental data does not bias the $\Delta\text{PDF}(r,t)$, we generate $\Delta\text{PDF}(r,t)$ for both the simulated averaged eq conformers and the experimental data, where we set the low s range to zero (see **Fig. S6**).

Theoretical Method:

AIMS simulations interfaced with GPU-accelerated α -CASSCF(23, 29-31) are used to model the photodynamics of isolated ax and eq rotamers of Φ -PH. The α -CASSCF has shown to be well-suited for this system based on our previous CHD work and single-point XMSPT2 calculations (**Fig. S7-9**).⁽²²⁾ Our active space consists of six electrons in four orbitals determined to minimize the average energy of the lowest two singlet states, within the 6-31G* basis set, i.e. α -SA-2-CASSCF(6,4)/6-31G*. Electronic structure calculations are performed with TeraChem.⁽³²⁻³⁴⁾ Following previous work, we use an α value of 0.82. A total of 90 initial conditions (15 sets of positions and momenta for each conformer) were selected from the computed electronic absorption spectrum (**Fig. S10**) and used to initiate the AIMS dynamics. The active-space molecular orbitals (MO) for all isomers were nearly identical to CHD (**Fig. S11**). These ICs are then placed on the S_1 surface and propagated with AIMS.

The first two singlet states (S_0 and S_1) are included in the dynamics. All required electronic structure quantities (energies, gradients, and nonadiabatic couplings) are calculated as needed with α -SA-2-CASSCF(6,4)/6-31G*. An adaptive timestep of 0.48 fs (20 au) (reduced to 0.12 fs (5 au) in regions with large nonadiabatic coupling) is used to propagate the centers of the trajectory basis functions (TBFs). A coupling threshold of 0.01 au (scalar product of nonadiabatic coupling and velocity vectors) demarcates spawning events generating new TBFs on different electronic states. Population transfer between TBFs is described by solving the time-dependent Schrödinger equation in the time-evolving TBF basis set.

We simulate the ultrafast dynamics for the first 1 ps of all six equatorial and axial conformational isomers of Φ -PH by: 1) using AIMS to propagate the initial wavepacket for the first 500 fs or until all population has returned to the ground state, 2) stopping TBFs on the ground state when they are decoupled from other TBFs (off-diagonal elements of the Hamiltonian become small), and 3) adiabatically continuing these stopped TBFs using the positions and momenta from the last frame in AIMS as initial conditions for adiabatic molecular dynamics with unrestricted DFT using the Perdew-Burke-Ernzerof hybrid exchange-correlation functional,⁽³⁵⁾ i.e. uPBE0/6-31G*. A total of 398 TBFs are propagated, with 306 of these being adiabatically continued on the ground state with DFT.

Simulation of modified molecular diffraction and pair distribution functions:

The $sM(s)$ simulations within the independent atom model (IAM) are generated from molecular geometries using a publicly available python code⁽³⁶⁾ and atomic scattering functions from the elsepa program.⁽³⁷⁾ PDFs are generated from the simulated $sM(s)$ using the same code as for the experimental data.

For the creation of ΔPDFs from the AIMS simulations, $sM(s)$ functions are evaluated for each time step of the simulation and each trajectory basis function (TBF) of a given initial condition separately both for the portion of the simulation using α -CASSCF and the extension on the ground state surface with DFT. The $sM(s)$ functions of different TBFs are averaged for each time step according to their population weights. The resulting averaged time-dependent $sM(s)$ functions are rebinned to 2 fs time steps. $\Delta sM(s, t)$ of a specific conformer are created by averaging the $sM(s, t)$ from all initial conditions of this conformer and

subtracting the initial $sM(s, t=0)$ function from the average. The $\Delta PDF(r, t)$ functions are created from $\Delta sM(s, t)$ functions using the same code as for the experimental $\Delta PDFs$. To account for the experimental response function, the $\Delta PDFs$ are convolved with a 150 fs FWHM Gaussian in time.

Supplementary Text

Supplementary note 1

We investigate the ground state potential energy surface using a number of different methods. A summary of our results can be found in **Fig. S12**. Our quantum chemical calculations find six possible αPH minimum geometries, three different rotamers for eq and ax geometries, which we label according to the $C_3-C_1-C_2-H_{ISO}$ dihedral angle of the isopropyl group shown in **Fig. 2** (i.e. gauche- (G-), trans (T), and gauche+ (G+)). Their S_0 minima are at $-58.5^\circ/-70.7^\circ$ (G-), $-172.9^\circ/179.4^\circ$ (T), and $57.0^\circ/48.9^\circ$ (G+) for ax/eq conformers, respectively. Our calculations find the eq- αPH minimum geometries to be in general more stable than ax- αPH and the thermal equilibrium, thus, dominated by similar fractions of the three eq- αPH rotamers. This is confirmed by a recent study on matrix isolated αPH which could only identify vibrational signatures of equatorial conformers.⁽²¹⁾

To quantify the possible amount of axial conformers in our gas phase sample, we fit a linear combination of the simulated $sM(s)$ functions of all six conformers to the experimental $sM(s)$. The coefficients of the axial conformer $sM(s)$ functions are always negative or zero if forced to be positive semidefinite. Thus, we cannot find any direct evidence for the presence of axial conformers in the static diffraction. We estimate the uncertainty of this assessment to be on the order of 10 %,

To quantify the contribution of ax- αPH ring-opening to the experimental signal, we create linear combinations of the averaged eq- αPH and ax- αPH and compare the time-dependence of the integrated α , β , and γ regions to the experimental data, analogous to **Fig. 3d**. A comparison using a linear combination with 20% ax- αPH contribution is plotted in **Fig. S13**. The α and β regions are only moderately sensitive to the fraction of ax- αPH contribution, since both ax- αPH and eq- αPH open the ring. As expected from **Fig. S3**, the γ -region is significantly more sensitive to the fraction of ax- αPH contribution. In **Fig. S13**, the intensity of the γ -signature is reduced far enough to be outside the error bars (68% confidence interval) of the experiment. Therefore, we estimate the contribution of ax- αPH to the time-dependent experimental signal to be <20%.

Supplementary note 2

In the AIMS simulations, we observe an additional photoproduct, 2-ladderane (5-isopropyl-2-methylbicyclo[2.2.0]hex-2-ene), which is formed in the electronic ground state exclusively by population having undergone internal conversion through the conical intersection CI-1. Since we do not observe internal conversion through CI-1 for the eq-G+ and ax-G- rotamers, the product is exclusively observed for the eq-T, eq-G-, ax-T, and ax-G+ rotamers (see **supplementary movies 1-4**). The ΔPDF signatures of 2-ladderane and ZEDOT are quite similar (see **Fig. S14**), especially in the γ -region. Additionally, the simulations predict only 5 % of the eq- α -phellandrene population undergoing internal conversion through CI-1 (see **Fig. 4** and **Table S1**). Therefore, a direct signature from the 2-ladderane contribution would be difficult to extract from the experimental data. However, it is included in the simulations and, therefore contributes to the quantitative agreement with experiment.

Supplementary Figures

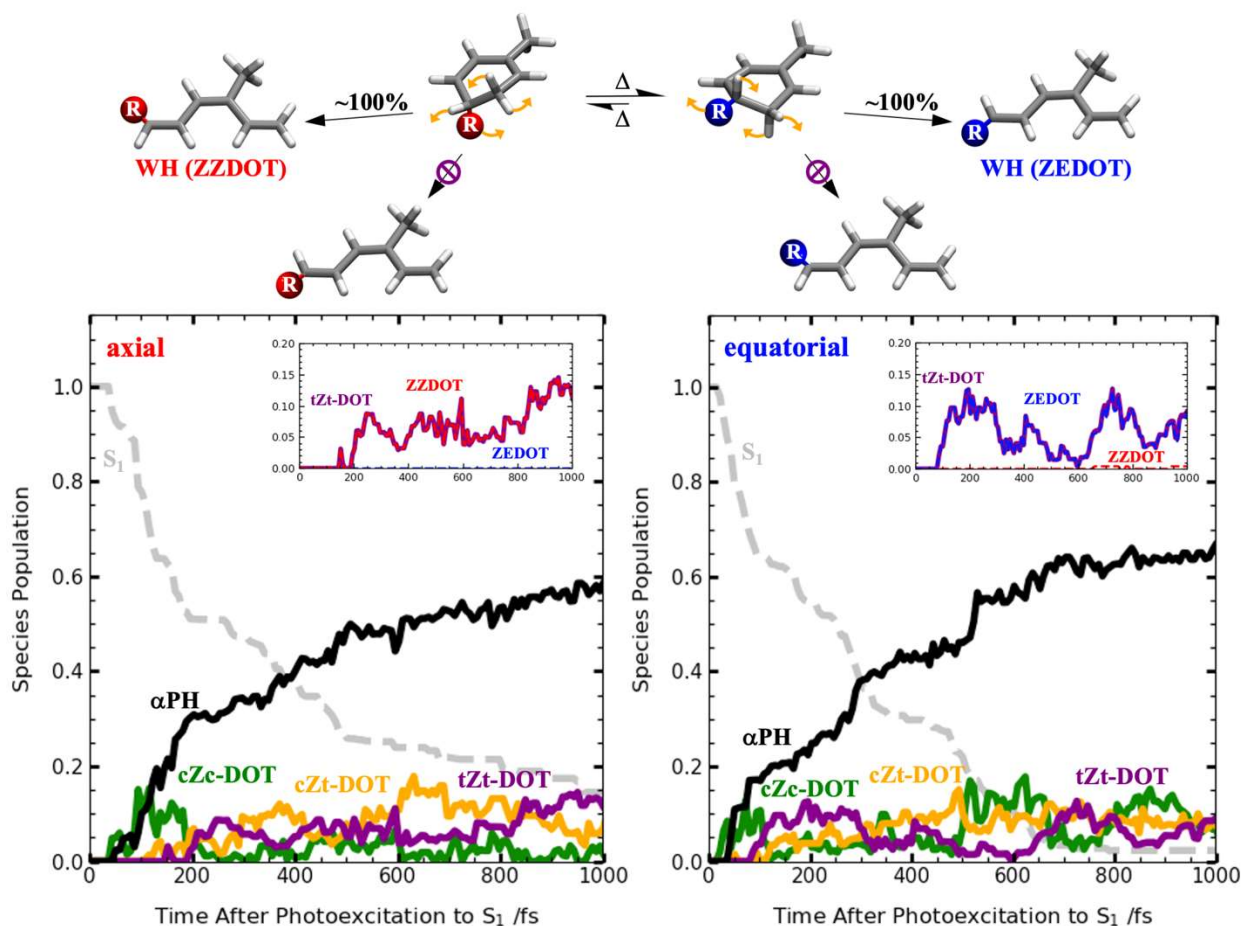


Fig. S1. AIMS Wavepacket Population for Axial and Equatorial Conformers. (Top) The Woodward-Hoffman allowed photoproducts from ax and eq α PH (the isopropyl group is represented as the R group). (Bottom) The wavepacket population from the axial (left) and equatorial (right) AIMS dynamics for the first picosecond after photoexcitation for all 90 ICs (45 each for ax and eq) considered. Snapshots every 5fs were binned based on the α PH, cZc, cZt, and tZt configurations and weighted according to their amplitudes. The insets show the tZt-DOT population decomposed into ZEDOT and ZDOT contributions for ax (left) and eq (right) photoproducts. Conrotatory ring-opening in the ax and eq ICs leads almost exclusively to the WH predicted ZEDOT (red) and ZDOT (blue) photoproducts, respectively.

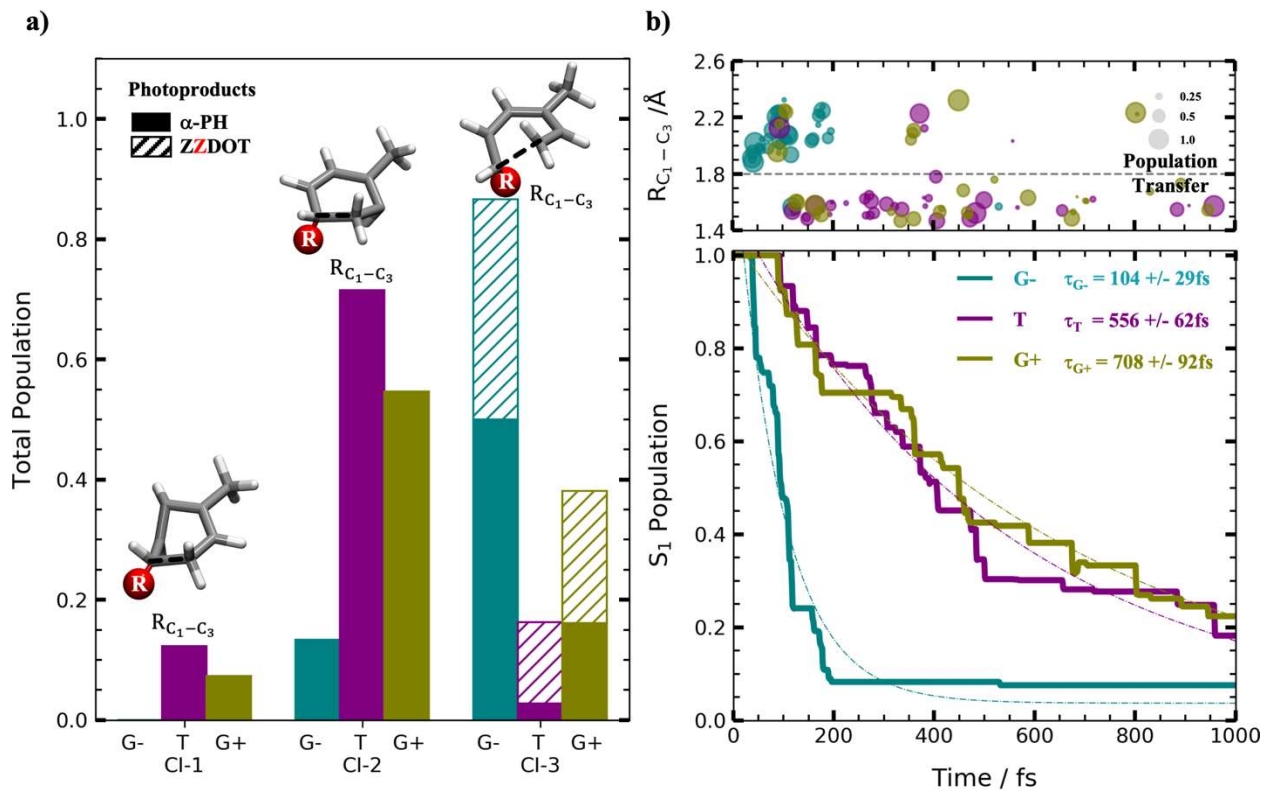


Fig. S2. Characterization of the Closed- and Open-Ring Nonradiative Relaxation Pathways for ax-Rotamers. a) A histogram of the branching ratio between the closed and open pathways from AIMS dynamics. Solid and striped bars represent fractional population that reformed α PH or cZc-ZDOT, respectively. b) (top) The C_1-C_3 distance vs spawning time for all 45 ax initial conditions. The black dashed line corresponds to the threshold used to determine if open or closed. The circle radius is proportional to the population transferred during the spawning event and separated into eq-G- (teal), eq-T (purple), and eq-G+ (olive). (bottom) The S_1 population decay for eq-G-, eq-T, and eq-G+ for the first ps after photoexcitation.

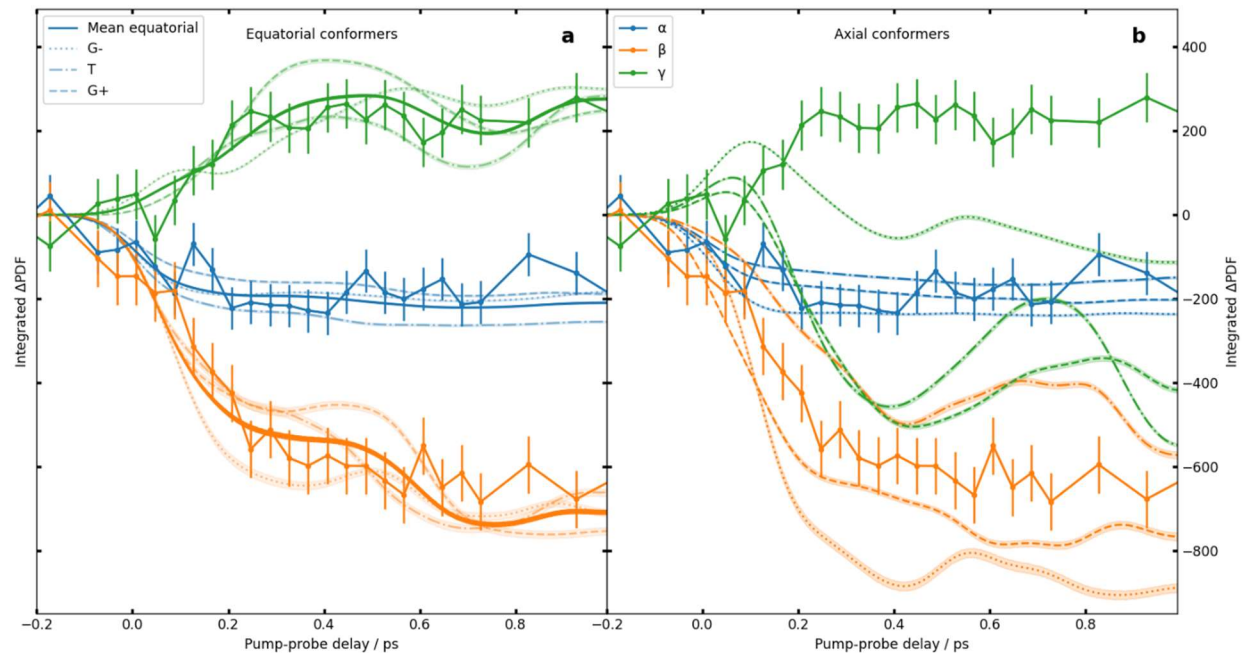


Fig. S3. Experimental and Simulated Signal Rise-Times Along Coordination Shells. (a) Temporal evolution of the integrated regions of the first (α , blue), second (β , orange) and third (γ , green) coordination shells of the experimental (connected points with error bars) and simulated Δ PDF averaged over the three equatorial rotamers (continuous lines). Simulated Δ PDF signals of the individual equatorial rotamers are shown as dotted (G-), dash-dotted (T), and dashed (G+) lines. The experimental data show quantitative agreement with the average of the simulated equatorial rotamer signals. (b) Analogous comparison between the experimental and simulated Δ PDF signals of the individual axial rotamers. Error bars represent a 68% confidence interval obtained from bootstrap analysis. The error bars of the simulations are visualized by the width of the lines and reflect convergence with respect to initial condition sampling.

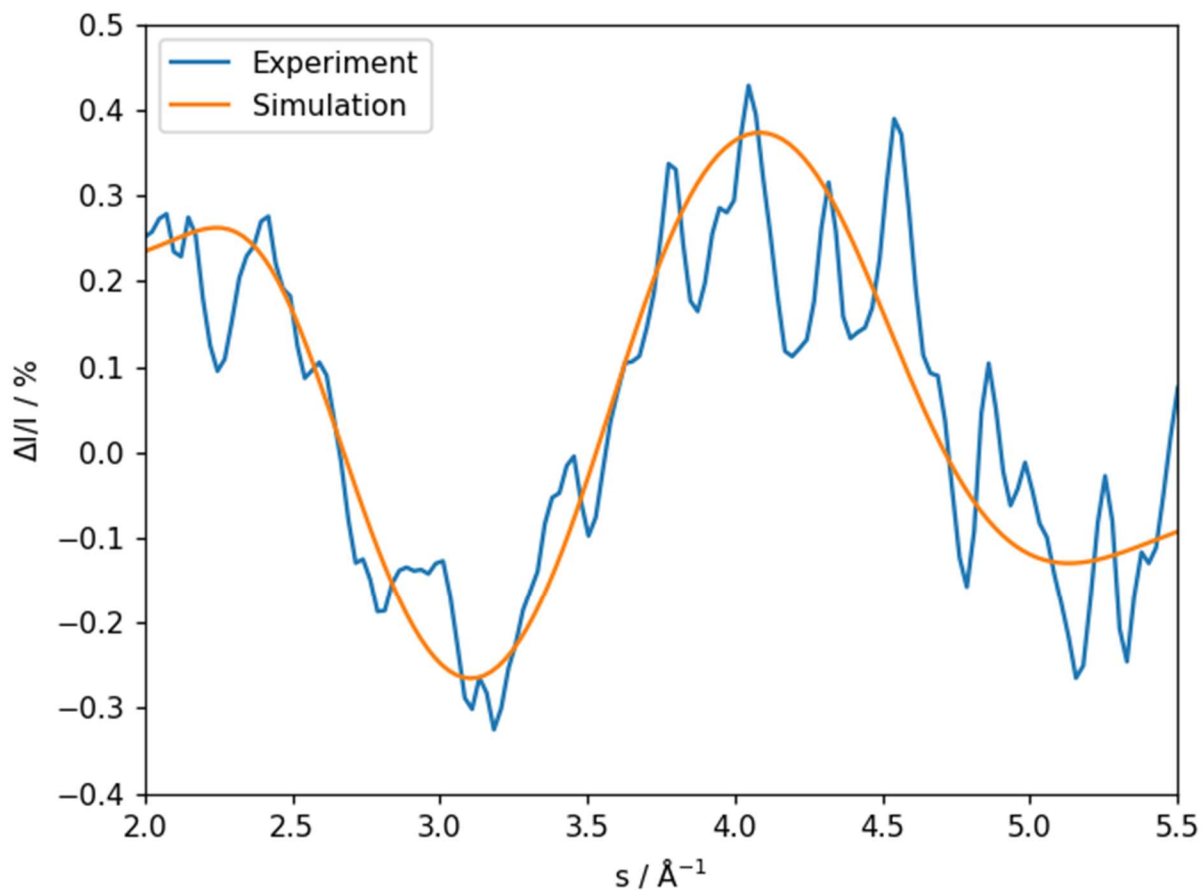


Fig. S4. Experimental and Simulated Relative Difference Diffraction Signals. Comparison between experimental and simulated relative difference diffraction signals $(I(1 \text{ ps}) - I(\text{steady-state})) / I(\text{steady-state})$. The simulation is scaled by a factor of 0.025 to match the amplitude of the experiment. This suggests an excitation ratio of 2.5 %.

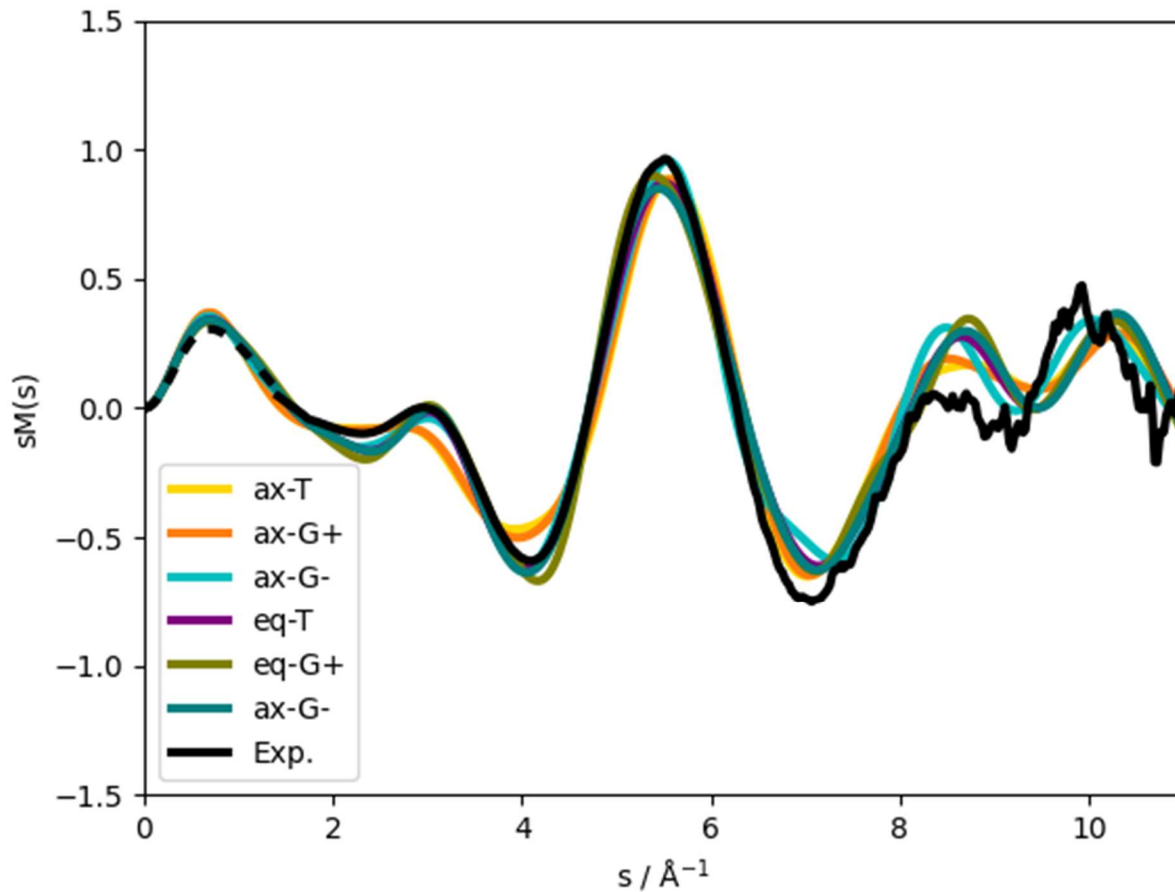


Fig. S5. Comparison of the experimental modified molecular diffraction $sM(s)$ with simulations of all six phellandrene conformers. The experimental $sM(s)$ is replaced by the average of the simulated $sM(s)$ below 1.5 \AA^{-1} to avoid artifacts from the hole in the detector in the experimental PDF (see Fig. 2a). As in Fig. 2a, we find good agreement between the experimental $sM(s)$ and four of the six possible conformers, all three equatorial and the ax-G- conformer, in a wide range from 1.5 \AA^{-1} to 8 \AA^{-1} . The agreement in Fig. 2a is worse in the range $>8 \text{ \AA}^{-1}$, which might be due to shortcomings in the subtraction of the atomic scattering background and limited signal-to-noise levels. The ax-T and ax-G+ conformers show significantly worse agreement with the experimental data in the region between 2 \AA^{-1} and 4.5 \AA^{-1} .

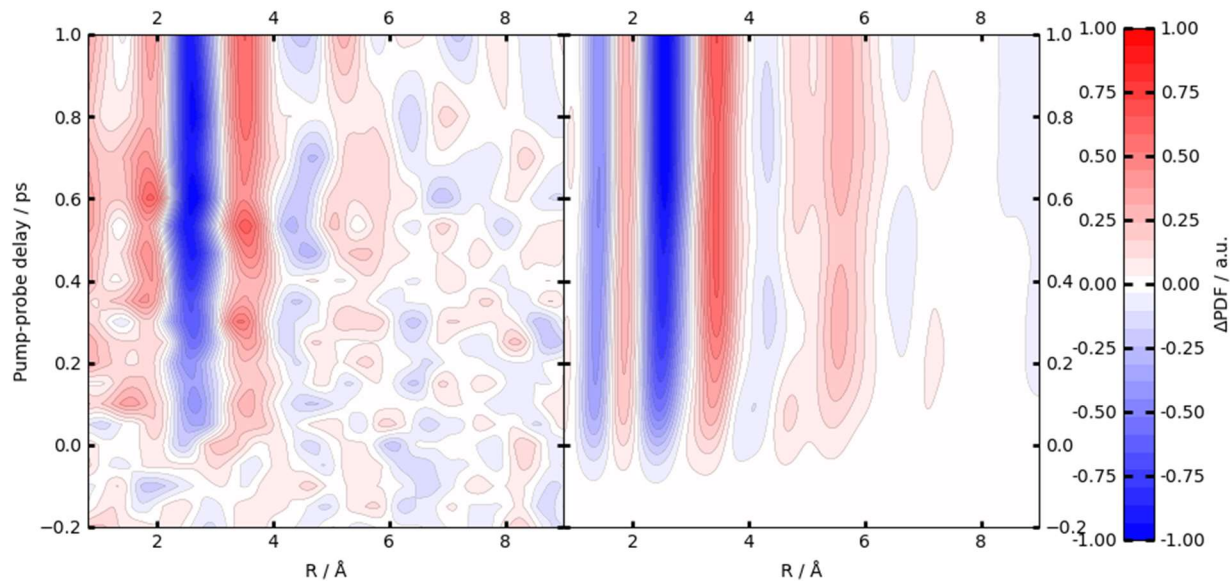


Fig. S6. Experimental $\Delta\text{PDF}(r,t)$ (left) and the average of the simulated $\Delta\text{PDF}(r,t)$ of equatorial rotamers (right) . Both $\Delta\text{PDF}(r,t)$ are generated while setting the s range $<0.6 \text{ \AA}^{-1}$ to zero to assess the bias to the experimental $\Delta\text{PDF}(r,t)$ by treatment of the $s < 0.6 \text{ \AA}^{-1}$ for Fig. 3 (see supplementary note 4). The main artifacts introduced by setting $s < 0.6 \text{ \AA}^{-1}$ to zero are a smooth positive contribution to distances $< 2 \text{ \AA}$ and a negative contribution to distances $> 4 \text{ \AA}$.

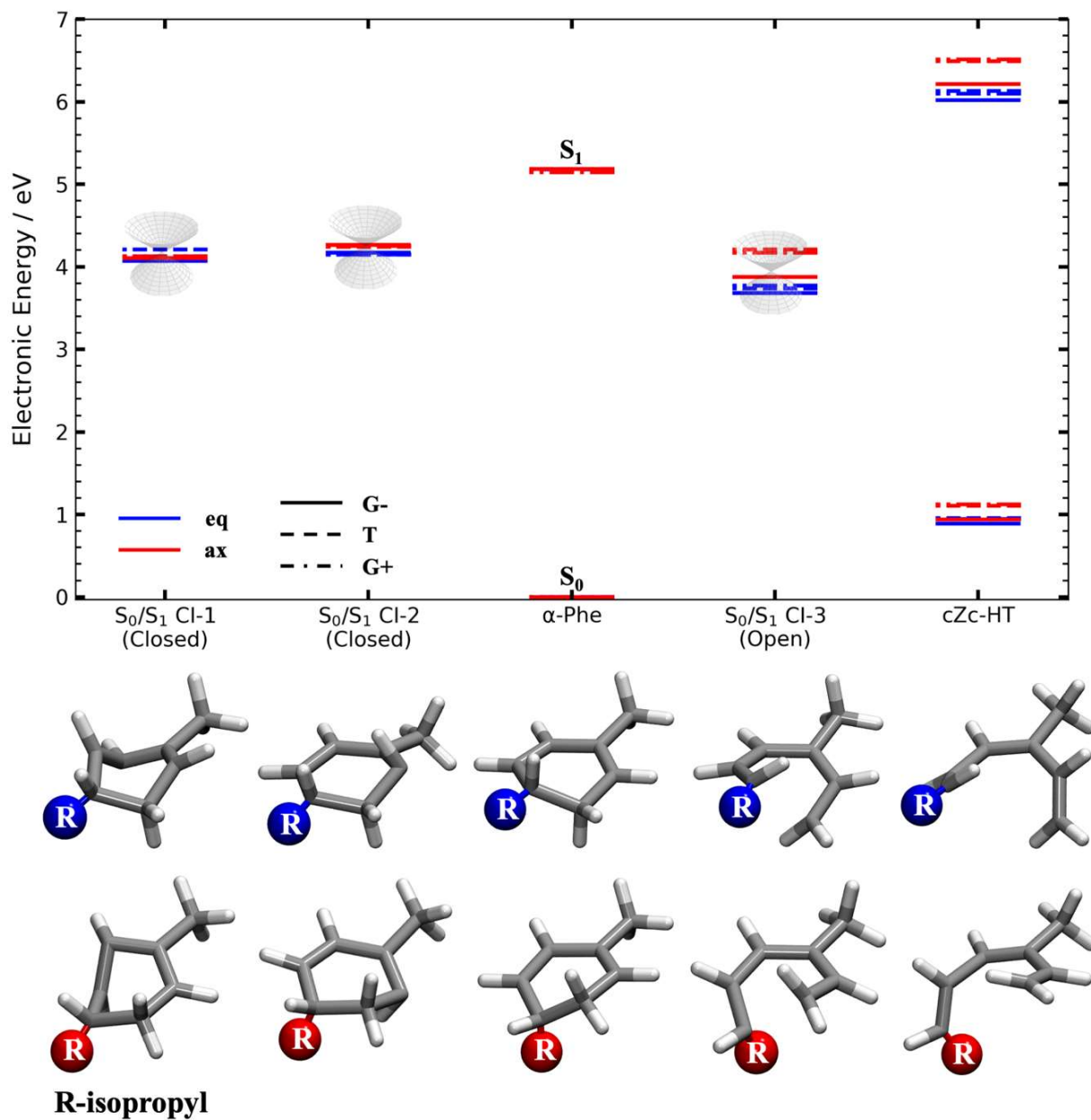


Fig. S7. Critical Points Along Nonradiative Relaxation Pathways in Ax and Eq α PH. The computed ax (red) and eq (blue) PESs at critical points along the OOP and ring-opening reaction coordinates in α PH. The energies are relative to each isomer's respective S_0 minimum ground-state energy. Geometries are shown in the bottom of the figure with the red (ax) and blue (eq) spheres representing the location of the ISO. Computed at the $\alpha(0.82)$ -SA2-CAS(6,4)-SCF/6-31G* level of theory. See **Table S2** for coordinates, energies, and CI vectors.

		G-		T		G+				G-		T		G+	
S_0 min	R_1 (Å)	1.53	1.54	1.53	1.54	1.53	1.54	cZc-HT	3.51	3.63	3.52	3.73	3.49	3.72	
	R_2 (Å)	2.82	2.82	2.82	2.83	2.82	2.83		3.18	3.15	3.18	3.15	3.18	3.15	
	R_3 (Å)	1.47	1.47	1.47	1.47	1.47	1.47		1.36	1.34	1.36	1.34	1.36	1.34	
	R_4 (Å)	4.36	3.59	4.36	3.85	4.36	3.81		4.71	3.67	4.70	4.04	4.70	4.09	
	R_5 (Å)	2.89	2.9	2.88	2.9	2.9	2.9		3.22	3.38	3.21	3.50	3.21	3.52	
	ω (°)	44.2	-46.7	43.4	-32.9	45.2	-35.2		71.7	-70.2	73.2	-61.2	72.7	-57.7	
	τ (°)	-70.7	-58.5	179.4	-172.9	48.9	57.0		-104.8	-52.3	133.2	168.1	17.2	53.5	
	α (°)	89.6	90.4	88.1	91.8	88.2	90.7		119.0	33.4	120.7	23.1	121.2	21.4	
	β (°)	92.3	88.4	92.2	89.8	92.0	88.9		47.5	114.0	46.7	106.1	48.4	103.4	
S_1/S_0 CI ₁	R_1 (Å)	1.54	1.55	1.53	1.54	1.54	1.54	S_1/S_0 CI ₃	2.28	2.13	2.27	2.15	2.23	2.12	
	R_2 (Å)	2.27	2.28	2.26	2.27	2.27	2.27		2.89	2.85	2.89	2.84	2.89	2.85	
	R_3 (Å)	1.39	1.40	1.38	1.39	1.39	1.39		1.41	1.38	1.41	1.39	1.41	1.39	
	R_4 (Å)	4.05	4.27	4.19	4.24	4.06	4.25		4.57	3.42	4.56	3.74	4.56	3.69	
	R_5 (Å)	2.96	2.9	2.96	2.9	3.0	2.9		3.06	3.0	3.06	3.1	3.1	3.08	
	ω (°)	20.3	-0.5	25.4	-13.8	20.6	-13.8		65.8	-66.9	65.4	-61.3	65.9	-62.0	
	τ (°)	-57.1	-53.9	179.1	-171.5	-52.01	57.3		-73.3	-52.6	-167.4	-164.4	14.6	63.1	
	α (°)	9.5	178.4	12.8	169.9	10.4	171.3		104.2	56.7	104.2	52.4	106.9	51.4	
	β (°)	79.0	97.5	78.1	99.2	79.4	98.6		69.7	117.1	69.2	118.0	68.9	117.4	

Fig. S8. The Structural Properties of the Critical Points. Computed structural properties of the critical points for all eq and ax isomers at the $\alpha(0.82)$ -SA2-CAS(6,4)-SCF/6-31G* level of theory. See Table S2 for coordinates, energies, and CI vectors.

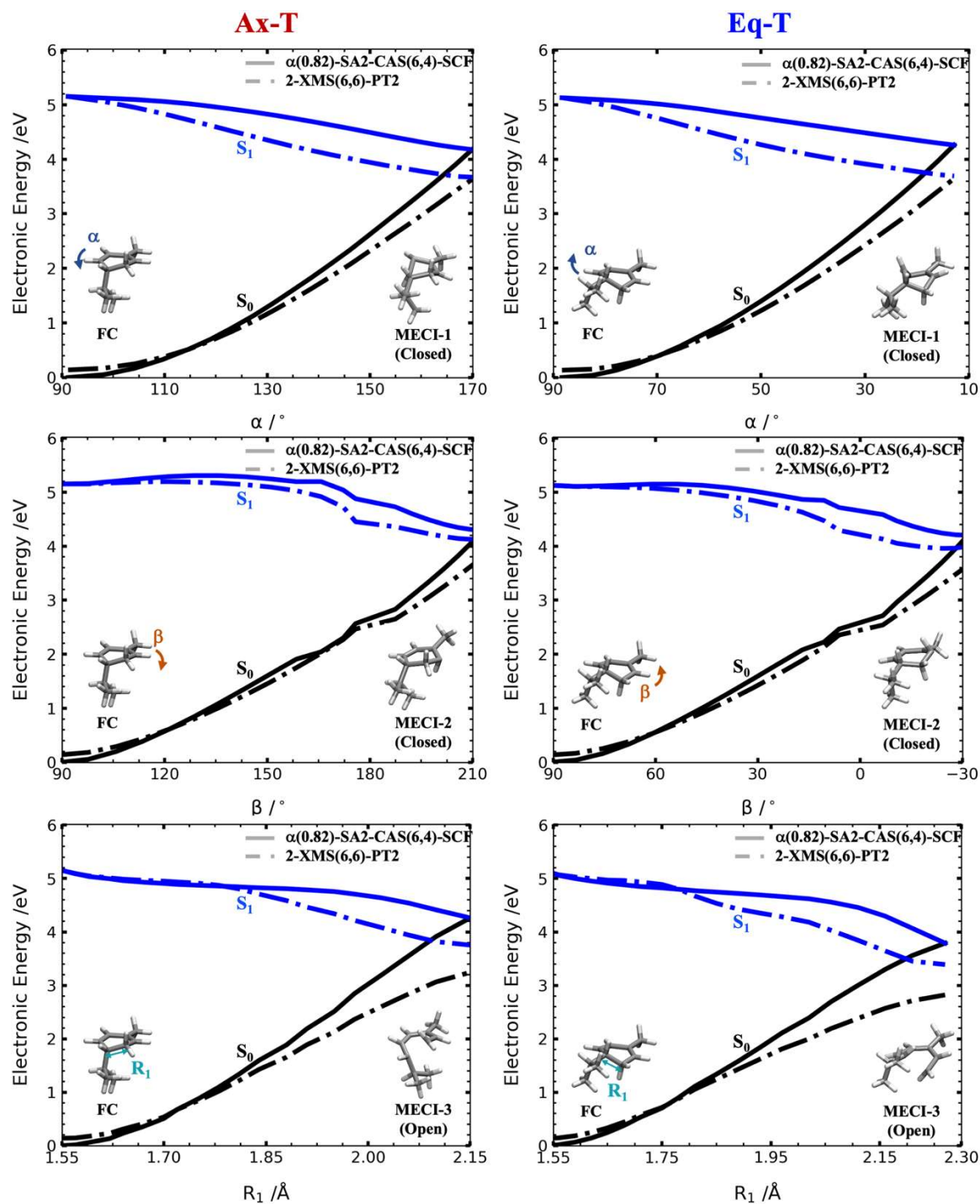


Fig. S9. Benchmarking α -SA-CASSCF Against XMSPT2 on S_1 with the G- Ax and Eq Conformers. Potential energy surface scans along the OOP (CI-1 and CI-2) and ring-opening (CI-3) coordinates on the S_1 electronic state. The pathways were generated from geodesic interpolation between the FC point and CI-1, CI-2, and CI-3 MECI structures, respectively, optimized at the $\alpha(0.82)$ -SA2-CAS(6,4)SCF/6-31G* level of theory and compared against single-point energy calculations with SA2-XMS-CAS(6,6)-PT2/6-31G*.

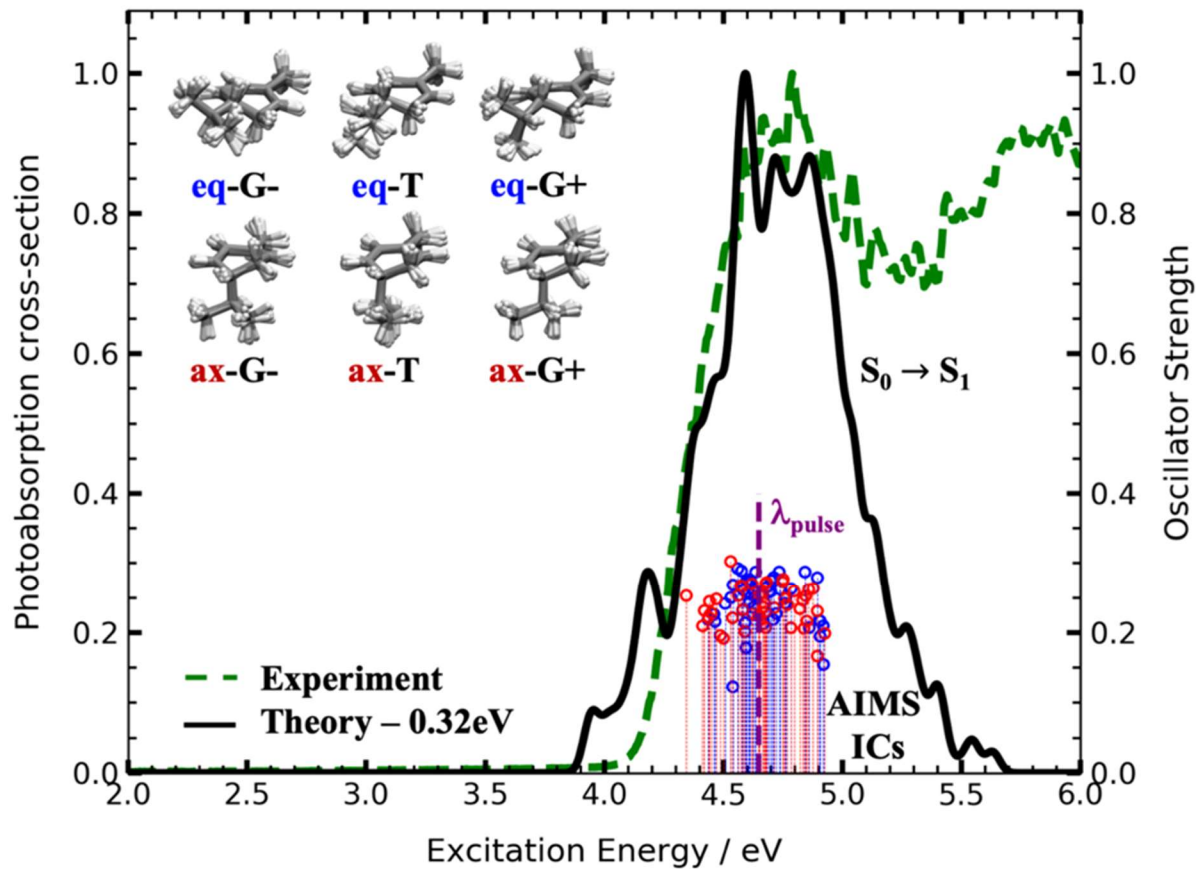


Fig. S10. UV Electronic Absorption Spectra of α PH: The UV electronic absorption spectrum was generated from 600 initial conditions sampled from a ground-state harmonic Wigner distribution. The AIMS dynamics simulations used 15 initial conditions for each conformer. The energy and oscillator strength for each of the initial conditions (randomly sampled with the restriction that they were within 0.3eV of the pump pulse energy used in the UED experiment) are shown with red/blue vertical lines for the axial/equatorial initial conditions respectively. The inset shows the starting geometries for each conformer.

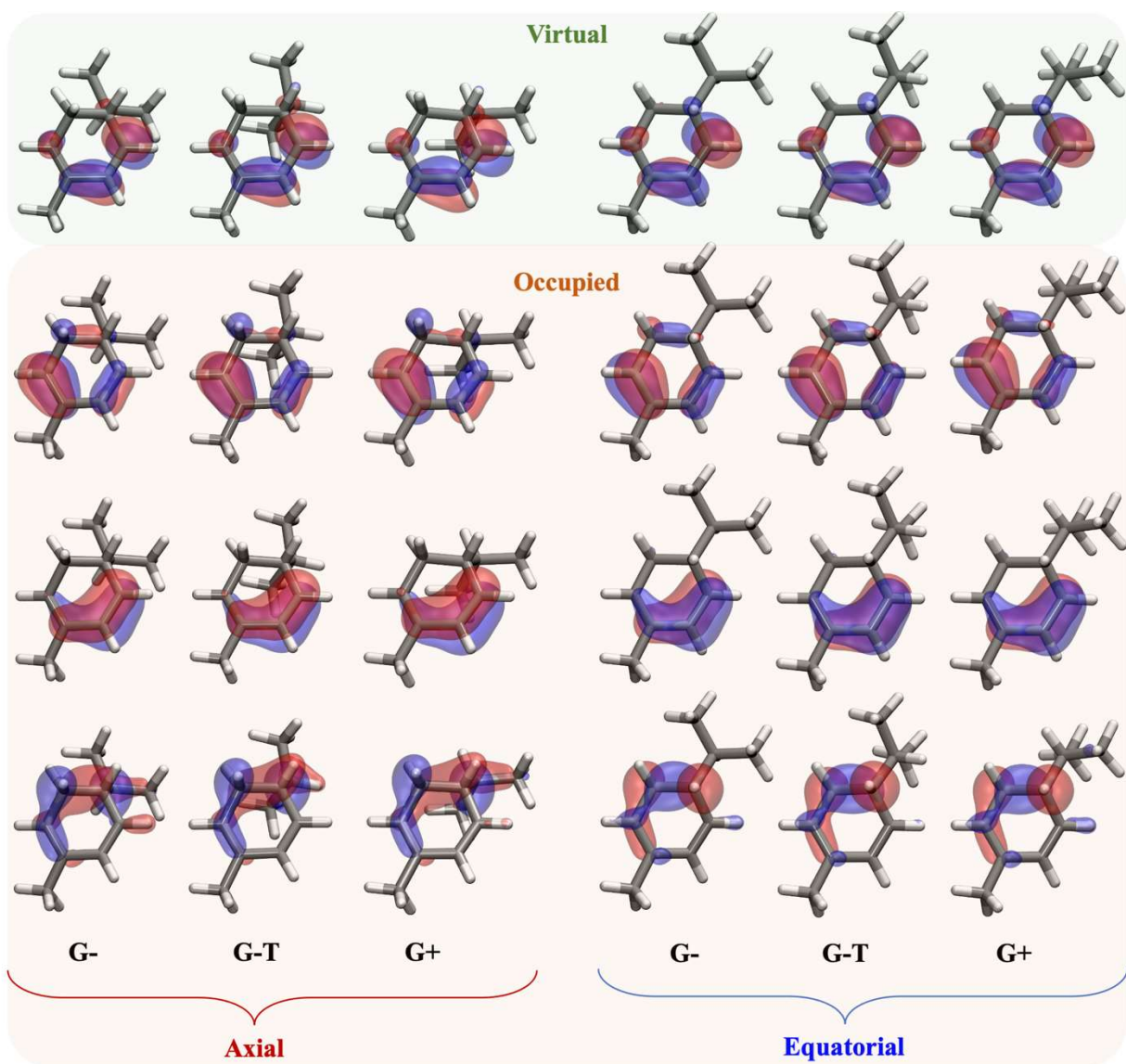
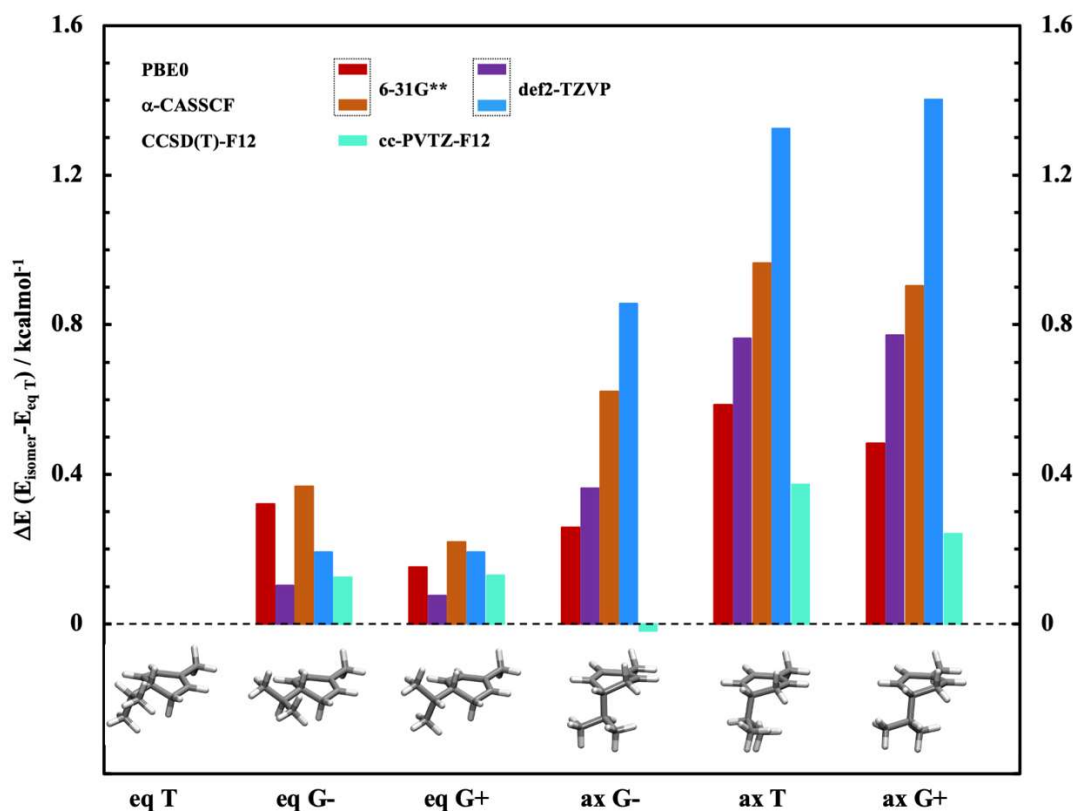


Fig. S11. SA-CASSCF Natural MOs at the S_0 Minima for all six aPH Isomers. The $\alpha(0.82)$ -SA2-CAS(6,4)SCF natural orbitals for the critical points along the α , β , and γ Z/E photoisomerization pathways. Blue and red correspond to 0.05 and -0.05 $e^{-/\text{\AA}^3}$ isovalues, respectively.



Method	Basis Set	$\Delta E (E_{\text{isomer}} - E_{\text{eq T}}) / \text{kcalmol}^{-1}$					
		eq T	eq G-	eq G+	ax G-	ax T	ax G+
PBE0	6-31G**	0.00	0.32	0.15	0.26	0.59	0.48
	def2-TZVP	0.00	0.10	0.08	0.36	0.76	0.77
α -CASSCF	6-31G**	0.00	0.37	0.22	0.62	0.96	0.90
	def2-TZVP	0.00	0.19	0.19	0.86	1.32	1.40
CCSD(T)-F12	cc-pVDZ-F12	0.00	0.12	0.13	-0.02	0.37	0.24

Fig. S12. The relative energies of the S_0 minima of the six most stable aPH isomers optimized at the PBE0/6-31G** level of theory and single-point energies computed with their labeled methods. α -CASSCF corresponds to a(0.82)-SA2-CAS(6,4)SCF. The aPH conformers are shown below their computed relative energies.

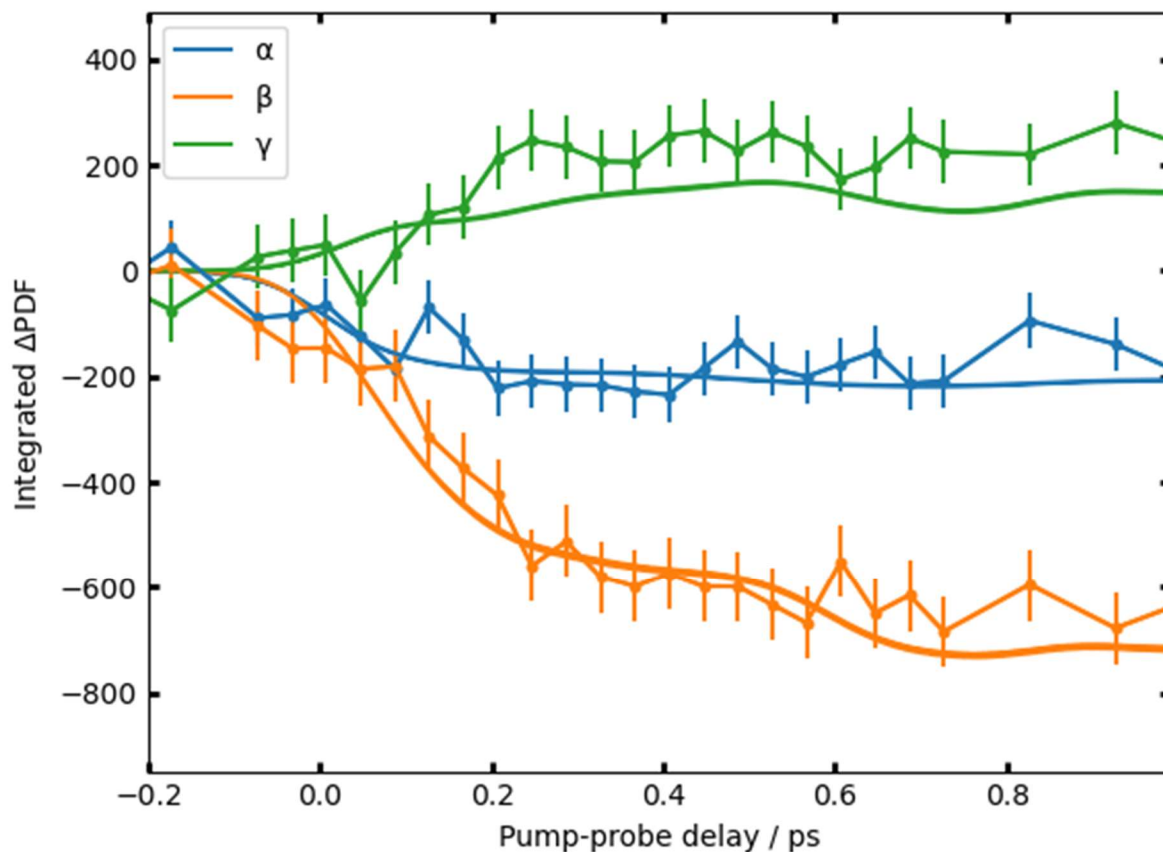


Fig. S13. Comparison of the experimental data to a linear combination of 80% eq- α PH and 20% ax- α PH, analogous to Fig. 3d. The intensity of the α and β features is not substantially changed by the linear combination, since both the eq- α PH and ax- α PH conformers open the ring. With a 20% contribution from ax- α PH, the intensity of the γ -signature reduced far enough (see Fig. S3) that the simulation is outside the error bars (68% confidence interval) of the experiment.

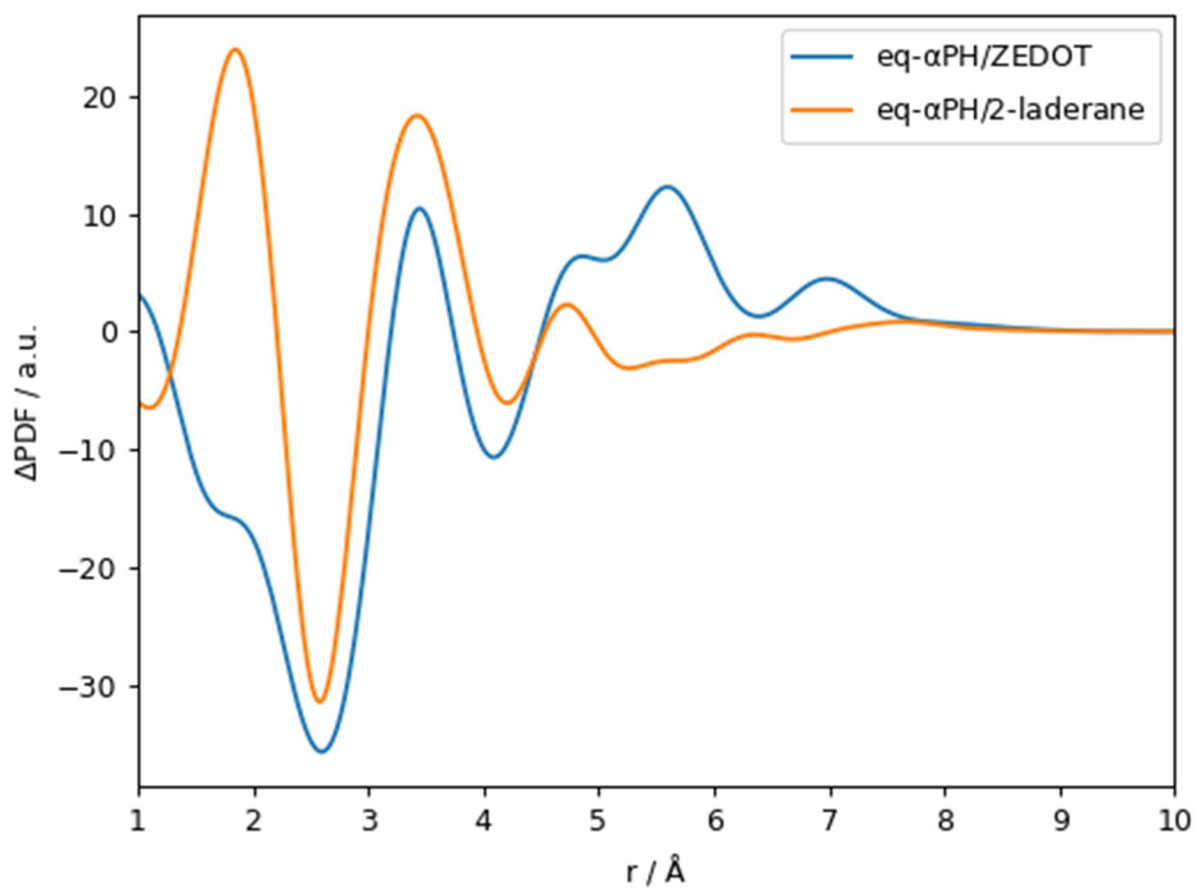
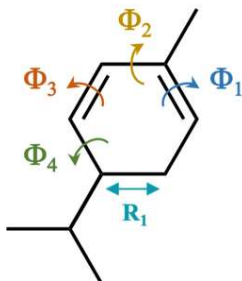


Fig. S14. Comparison of simulated ΔPDF signatures of the ZEDOT and 2-ladderane photoproducts. The ΔPDF signatures are generated analogous to **Fig. 2**.

Supplementary Tables

Isomer	CI-1 (%)		CI-2 (%)		CI-3 (%)	
	α PH	<i>ZZ/ZE</i> -DOT	α PH	<i>ZZ/ZE</i> DOT	α PH	<i>ZZ/ZE</i> -DOT
Axial	6 +/- 2	0	46 +/- 5	0	24 +/- 4	24 +/- 4
G-	0	0	13 +/- 6	0	50 +/- 7	37 +/- 6
T	12 +/- 6	0	71 +/- 8	0	3 +/- 1	14 +/- 6
G+	7 +/- 3	0	55 +/- 9	0	17 +/- 5	21 +/- 7
Equatorial	5 +/- 2	0	35 +/- 4	0	30 +/- 3	30 +/- 3
G-	9 +/- 4	< 1	22 +/- 6	0	38 +/- 7	31 +/- 6
T	6 +/- 2	0	34 +/- 8	0	30 +/- 6	30 +/- 6
G+	0	0	50 +/- 8	0	21 +/- 5	29 +/- 6

Table S1. Computed Quantum Yield for Eq and Ax α PH. The computed quantum yields for ax (red) and eq (blue) α PH from the AIMS simulation. Errors represent a 68% confidence interval and obtained from bootstrap analysis. The geometries associated with each CI are included in the supplementary structures.



Conformer	R_1 (Å)	$ \Phi_1 $ (°)	$ \Phi_2 $ (°)	$ \Phi_3 $ (°)	$ \Phi_4 $ (°)
α PH	≤ 1.8	≤ 80	≤ 80	≤ 80	-
cZc DOT	> 1.8	≤ 80	≤ 80	≤ 80	-
cZt/tZc DOT	> 1.8	≤ 80 or ≥ 100	≤ 80	≥ 100 or ≤ 80	-
tZt DOT	> 1.8	≥ 100	≤ 80	≥ 100	-
ZZ DOT	> 1.8	≥ 100	≤ 80	≥ 100	≤ 80
ZE DOT	> 1.8	≥ 100	≤ 80	≥ 100	≥ 100

Table S2. Binning criteria for aPH conformers upon relaxation to the ground-electronic state. Each row corresponds to a specific conformer along with the structural parameters used to classify a specific geometry R(t). The carbon-carbon distance (R_1), and the absolute values of the four dihedral angles (F_1 , F_2 , F_3 , and F_4) are shown above on the aPH structure.

ax-G- S₀ Minimum (FC)

Cartesian coordinates / 26

Å

C	0.5603236327	0.4023961588	-0.7534127770
C	0.7083580082	0.2280638902	-2.2917607550
C	-0.4806859329	1.4601042097	-0.3427323697
C	0.1905270201	-0.9037782124	-0.0835836769
C	1.1561432757	1.5217719416	-2.9836108245
C	1.6972509320	-0.8934076400	-2.6346771681
C	-1.8966775403	0.9530193094	-0.4431649948
C	-2.1892619383	-0.3262247477	-0.1896019727
C	-1.1016287345	-1.2366900564	0.1308329124
C	-3.5971279122	-0.8637417517	-0.1983626931
H	1.5295358649	0.7243728535	-0.3774203022
H	-0.2652108994	-0.0513786141	-2.6868248926
H	-0.3612853868	2.3725422211	-0.9128206563
H	-0.2910190030	1.7300974998	0.6974986094
H	0.9717223103	-1.6003674665	0.1631218703
H	2.0942398065	1.8821564697	-2.5675740747
H	1.3142229773	1.3480004559	-4.0437769645
H	0.4259905321	2.3174470212	-2.8965062503
H	2.6834867910	-0.6825871333	-2.2264033648
H	1.8034611151	-0.9919160193	-3.7107171621
H	1.3735024045	-1.8532756844	-2.2505699153
H	-2.6788309627	1.6577899201	-0.6692289336
H	-1.3468031635	-2.2011433469	0.5430824664
H	-4.3167380410	-0.0869263586	-0.4286740953
H	-3.8554407042	-1.2860978305	0.7695949806
H	-3.7080644517	-1.6572470888	-0.9328169955

S₀ energy / H -387.96054165320811
 S₀ CI eigenvector
 -0.97504331747285 X36 X37 X38
 0.11393573558125 X36 X37 X39
 0.09694743023016 X36 X37 A38 B39
 0.09694743023016 X36 X37 B38 A39
 0.08914326689277 X36 X38 X39
 -0.05944949541773 X36 A37 B38 X39
 -0.05944949541773 X36 B37 A38 X39
 -0.02940805078553 A36 X37 B38 X39
 -0.02940805078553 B36 X37 A38 X39

S₁ energy / H -387.77196192146300
 S₁ CI eigenvector
 0.66569875346325 X36 X37 A38 B39
 0.66569875346325 X36 X37 B38 A39
 0.16659600268016 X36 A37 X38 B39
 0.16659600268016 X36 B37 X38 A39
 0.14470360526893 X36 X37 X39
 0.13321696755136 X36 X37 X38
 -0.10551863283796 X36 X38 X39
 0.04302315766171 X36 A37 B38 X39
 0.04302315766171 X36 B37 A38 X39
 -0.03902941742766 A36 X37 B38 X39
 -0.03902941742766 B36 X37 A38 X39
 0.02509392450520 A36 X37 X38 B39
 0.02509392450520 B36 X37 X38 A39

ax-G- S₁/S₀ MECI-1 (Closed)

Cartesian coordinates / 26
 Å
 C 0.1621130953 0.3955961655 -1.1141988442
 C 0.7554693358 0.4585408063 -2.5301436349

C	-0.9982808394	1.3903029991	-0.8564786760
C	-0.5200554079	-0.8934853963	-0.7580407137
C	1.4207136966	1.8157466977	-2.7849453037
C	1.7662869611	-0.6692895249	-2.7708141217
C	-2.2081768506	0.6026907689	-0.4024733111
C	-2.1335035690	-0.4945820310	0.4651025289
C	-0.9020356518	-1.1433888871	0.6157552912
C	-3.4055396165	-1.0750878568	1.0361741662
H	0.9494501058	0.5417641763	-0.3790014621
H	-0.0620339365	0.3377675863	-3.2405277112
H	-1.2455509581	1.8841126506	-1.7897108748
H	-0.7295990292	2.1744307534	-0.1492908892
H	-0.7957838139	-1.5654818326	-1.5618515905
H	2.2390688093	1.9789179397	-2.0885236535
H	1.8288636695	1.8626898754	-3.7897525351
H	0.7259965935	2.6411199744	-2.6750474642
H	2.6222121244	-0.5717508947	-2.1085328887
H	2.1334163496	-0.6449568693	-3.7922160811
H	1.3351328597	-1.6522678531	-2.6068862224
H	-3.1783057381	1.0133707489	-0.6255953245
H	-0.8978478290	-2.1402797112	1.0182670790
H	-3.8378633989	-1.7899590253	0.3425576005
H	-4.1407189015	-0.2999167599	1.2253504958
H	-3.1938291008	-1.5950621513	1.9626938446

So energy / H -387.80784501018326

So CI eigenvector 0.64709438890734 X36 X37 A38 B39

0.64709438890734 X36 X37 B38 A39

0.34695217065350 X36 X37 X38

-0.12074460502525 X36 A37 B38 X39

-0.12074460502525 X36 B37 A38 X39
0.07475597349097 X36 A37 X38 B39
0.07475597349097 X36 B37 X38 A39
-0.03931498098687 X36 X38 X39

S₁ energy / H -387.80784494827003

S₁ CI eigenvector 0.91822500256939 X36 X37 X38
-0.24880197931689 X36 X37 A38 B39
-0.24880197931689 X36 X37 B38 A39
-0.09515242037606 X36 X38 X39
0.08644154315953 X36 A37 X38 B39
0.08644154315953 X36 B37 X38 A39
0.05692936396372 X36 A37 B38 X39
0.05692936396372 X36 B37 A38 X39
-0.03993705200290 X37 X38 X39
-0.02522895954515 X36 X37 X39

ax-G- S₁/S₀ MECI-2 (Closed)

Cartesian coordinates / 26
Å

C 0.2778394844 0.7402758905 -0.9436995820
C 0.6503719408 0.2715291507 -2.3871127407
C -1.0396062394 1.5584442046 -0.8519567648
C 0.1842609901 -0.4772280282 -0.0541691708
C 0.6567092825 1.4346682168 -3.3863680272
C 2.0183001147 -0.4274011723 -2.4178296436
C -2.3414841531 0.7087306843 -0.8612023319
C -2.2141956516 -0.3553061164 0.0641837175

C	-0.9600545966	-1.0705232758	0.3100330113
C	-3.4061451847	-0.7973599899	0.8573050918
H	1.1179291181	1.3429610916	-0.5972064999
H	-0.0958012795	-0.4474428770	-2.7161738790
H	-1.0688533166	2.3007857938	-1.6353233566
H	-1.0285218047	2.1194928466	0.0803919283
H	1.1078654787	-0.9194881186	0.2793939825
H	1.2757531546	2.2543892213	-3.0301579862
H	1.0621302520	1.1067821862	-4.3384028664
H	-0.3369049217	1.8191988087	-3.5744596838
H	2.8050280313	0.2412133230	-2.0767374427
H	2.2643399127	-0.7320552651	-3.4299009112
H	2.0493782122	-1.3194550302	-1.8017253245
H	-1.9867231265	-0.0617963457	-1.6329539545
H	-0.9436437217	-1.9469927486	0.9350040700
H	-3.9033571669	0.0926770406	1.2255139528
H	-3.1809887850	-1.4927685603	1.6583762018
H	-4.0991488352	-1.2694627991	0.1673533469

So energy / H -387.80197661779243

So Cl eigenvector 0.61288824429786 X36 X37 A38 B39
0.61288824429786 X36 X37 B38 A39
-0.47210234524164 X36 X37 X38
-0.07823966371266 X36 A37 B38 X39
-0.07823966371266 X36 B37 A38 X39
0.05200492398262 A36 X37 B38 X39
0.05200492398262 B36 X37 A38 X39
-0.05053978461282 X36 A37 X38 B39
-0.05053978461282 X36 B37 X38 A39
0.03900987873768 X36 X38 X39

0.03798693530241 X37 X38 X39

S₁ energy / H -387.80197656569987

S₁ CI eigenvector -0.86047987680726 X36 X37 X38

-0.33611040007945 X36 X37 A38 B39

-0.33611040007945 X36 X37 B38 A39

-0.09283438295822 X36 A37 X38 B39

-0.09283438295822 X36 B37 X38 A39

0.07457338036087 X36 X38 X39

0.05910489653625 X37 X38 X39

0.03898805618125 X36 A37 B38 X39

0.03898805618125 X36 B37 A38 X39

-0.03054638312189 A36 X37 B38 X39

-0.03054638312189 B36 X37 A38 X39

0.03000672656738 A36 X37 X38 B

ax-G- S₁/S₀ MECI-3 (Open)

Cartesian coordinates /

Å

26

C 0.8417220268 0.3094150283 -0.7527754442

C 0.6684700878 0.2214409531 -2.2643079427

C -0.6958979840 1.6461909802 -0.1426474445

C 0.2844862496 -0.6297399299 0.1341828001

C 0.9992342452 1.5374316838 -2.9762029416

C 1.5616871132 -0.9016635253 -2.8201445510

C -1.8763693304 1.0561312980 -0.6336239893

C -2.1094764742 -0.3083304716 -0.3426723474

C -1.0710316514 -1.1015591199 0.1157619641

C -3.5023331242 -0.8672701793 -0.4822571987

H 1.8136285935 0.6807553281 -0.4577909945

H -0.3608848334 -0.0334349404 -2.4824666315

H	-0.3559649374	2.5761288705	-0.5647945372
H	-0.4631322682	1.5528539700	0.9031165436
H	0.8851773650	-0.9178316287	0.9866735061
H	2.0128804599	1.8602113593	-2.7513681460
H	0.9263962167	1.4154061612	-4.0529847435
H	0.3226519642	2.3354558845	-2.6941835457
H	2.6122420179	-0.6942201329	-2.6317535898
H	1.4349543141	-1.0013416331	-3.8953038697
H	1.3229835357	-1.8563926264	-2.3635138377
H	-2.4347179111	1.5415274257	-1.4141879774
H	-1.2872180516	-2.0506155676	0.5759124282
H	-4.0695445146	-0.6663727822	0.4229638103
H	-3.4986832287	-1.9374193803	-0.6527548730
H	-4.0278662559	-0.3845268228	-1.2992176941

S₀ energy / H -387.81621596389630

S₀ CI eigenvector

-0.68422866365199	X36	X37	A38	B39
-0.68422866365199	X36	X37	B38	A39
-0.20802236504258	X36	X37	X38	
0.06916271094306	X36	A37	B38	X39
0.06916271094306	X36	B37	A38	X39
0.06569307897616	A36	X37	B38	X39
0.06569307897616	B36	X37	A38	X39
0.03658466309883	X36	X38	X39	

S₁ energy / H -387.81621591282703

S₁ CI eigenvector

0.95912177525701	X36	X37	X38	
-0.14830333425409	X36	X37	A38	B39
-0.14830333425409	X36	X37	B38	A39
-0.12097924030911	X37	X38	X39	

-0.10079638786795 X36 X38 X39
0.06150863043967 X36 X37 X39
0.04052344337378 X36 A37 X38 B39
0.04052344337378 X36 B37 X38 A39
0.03600610810151 A36 X37 X38 B39
0.03600610810151 B36 X37 X38 A39
-0.02612209225221 A36 B37 X38 X39
-0.02612209225221 B36 A37 X38 X39

ax-G- cZc-ZDOT Minimum

Cartesian coordinates / 26
Å

C 1.3090863484 -0.5878350482 -0.7434429896
C 1.0465692236 -0.7793383837 -2.2162131453
C -1.1432254930 2.0674572329 -0.3657589622
C 0.4441091090 -0.6690636364 0.2553290459
C 1.4842781081 0.4594064191 -3.0084413775
C 1.7748265009 -2.0329293034 -2.7220502343
C -1.9719833495 1.0816773488 -0.7649518194
C -2.0283354018 -0.2931430453 -0.2757166191
C -0.9959479244 -1.0165419993 0.1787065913
C -3.4109996727 -0.9102520116 -0.3126350699
H 2.3385346354 -0.3788405082 -0.4902012134
H -0.0175593621 -0.9206312376 -2.3640545539
H -1.2235225903 3.0521754435 -0.7893540989
H -0.3877864618 1.9206509692 0.3811859555
H 0.8284274383 -0.5527355098 1.2586502807
H 2.5488757139 0.6441614973 -2.8867486787
H 1.2924245572 0.3254287432 -4.0691429647

-0.11706601371077 X36 X37 X38
0.09710454236041 A36 X37 X38 B39
0.09710454236041 B36 X37 X38 A39
0.08284563231944 X36 X38 X39
0.06809940224884 A36 B37 X38 X39
0.06809940224884 B36 A37 X38 X39
0.04489481348085 A36 X37 B38 X39
0.04489481348085 B36 X37 A38 X39
0.03636524577451 X37 X38 X39

ax-T S₀ Minimum (FC)

Cartesian coordinates / 26
Å

C	0.4502477944	0.3858873308	-0.8255864458
C	0.7687565070	0.2731381052	-2.3441796670
C	-0.6076555934	1.4488225252	-0.4521150388
C	0.0835415899	-0.9600552283	-0.2479503836
C	-0.4571367087	0.0115373802	-3.2238624198
C	1.5524508023	1.4890979255	-2.8518281417
C	-2.0159393139	0.9246941880	-0.3377482764
C	-2.2834354747	-0.3509479971	-0.0496991026
C	-1.1812343315	-1.2891203307	0.0888161116
C	-3.6866917326	-0.8672761375	0.1401144469
H	1.3846777604	0.6900663308	-0.3597431961
H	1.4270606391	-0.5888336735	-2.4443582508
H	-0.5798836275	2.2771280132	-1.1520149567
H	-0.3371222547	1.8755561345	0.5141255427
H	0.8700396515	-1.6902880218	-0.1592491233
H	-1.1291658999	0.8640272239	-3.2373739503

0.04697596455500 X36 A37 B38 X39

0.04697596455500 X36 B37 A38 X39

0.03705590102833 A36 X37 B38 X39

0.03705590102833 B36 X37 A38 X39

ax-T S₁/S₀ MECI-2 (Closed)

Cartesian coordinates / 26

Å

C	0.1808644782	0.4500345681	-1.0668957398
C	0.7306901804	0.4416699246	-2.5058899281
C	-0.9829282960	1.4208801042	-0.7826467665
C	-0.4381036175	-0.8472752336	-0.6259978323
C	-0.3326682595	0.2274610726	-3.5901252213
C	1.5327951603	1.7166074448	-2.7840262730
C	-2.2117374626	0.5646794218	-0.5562637724
C	-2.1891123592	-0.4507695297	0.4309142767
C	-0.9494181186	-1.0030989701	0.7224953486
C	-3.4824466097	-1.0271946217	0.9467804728
H	1.0117094401	0.6391196786	-0.3859767902
H	1.4268204076	-0.3954272541	-2.5637397676
H	-1.1399214090	2.0923670604	-1.6169514010
H	-0.7745655244	2.0424358630	0.0881733393
H	-0.4454872489	-1.6854188197	-1.3093100023
H	-1.0214143992	1.0636226718	-3.6468541643
H	0.1434552956	0.1320520463	-4.5613210902
H	-0.9210161497	-0.6665709663	-3.4189634304
H	0.9088260499	2.6009700121	-2.6971309000
H	1.9423490954	1.7041018794	-3.7893597243
H	2.3596023127	1.8232361887	-2.0882471015

H	-3.1628201341	0.8978374660	-0.9351446585
H	-0.8841031802	-1.9433254484	1.2378430318
H	-3.8865408308	-1.7343607638	0.2286516487
H	-4.2189872313	-0.2438387243	1.0937466728
H	-3.3235911130	-1.5493832365	1.8823656843

S_0 energy / H	-387.80647282293432
S_0 CI eigenvector	-0.59113790085849 X36 X37 A38 B39
	-0.59113790085849 X36 X37 B38 A39
	0.51556069399260 X36 X37 X38
	0.11745014710862 X36 A37 B38 X39
	0.11745014710862 X36 B37 A38 X39
	-0.06060959378354 X36 X38 X39
	0.04043277310390 X36 A37 X38 B39
	0.04043277310390 X36 B37 X38 A39
	-0.02238637587029 X37 X38 X39

S_1 energy / H	-387.80647265599879
S_1 CI eigenvector	-0.83395067122596 X36 X37 X38
	-0.36275405473977 X36 X37 A38 B39
	-0.36275405473977 X36 X37 B38 A39
	-0.10455299633048 X36 A37 X38 B39
	-0.10455299633048 X36 B37 X38 A39
	0.09196027125666 X36 X38 X39
	0.06801797704185 X36 A37 B38 X39
	0.06801797704185 X36 B37 A38 X39

Cartesian coordinates / 26

Å

C	0.3825027852	0.4227521758	-0.8695869794
C	0.9825591475	0.2774215461	-2.3001824496
C	-0.7345064912	1.5038137890	-0.7247397624
C	-0.0544360883	-0.9383149088	-0.3781330739
C	-0.0509064085	-0.0303514342	-3.3894865337
C	1.8159616934	1.5067801491	-2.6777693529
C	-2.1972186461	0.9933194355	-0.6416488270
C	-2.3018615671	-0.2183401653	0.0768021812
C	-1.2881109985	-1.2836106789	-0.0115475886
C	-3.5024456664	-0.5108005602	0.9254816919
H	1.2307323963	0.6974915081	-0.2424082460
H	1.6730486977	-0.5649883173	-2.2619720432
H	-0.6608633583	2.2147958570	-1.5360841287
H	-0.5458803302	2.0752356565	0.1791964595
H	0.7183790077	-1.6902556425	-0.3373438151
H	-0.7414920618	0.7943437359	-3.5271475416
H	0.4476300772	-0.1992868816	-4.3395103268
H	-0.6301688817	-0.9200618565	-3.1623629051
H	1.2018960046	2.3943282812	-2.7865742496
H	2.3252935260	1.3432384308	-3.6226938174
H	2.5720026887	1.7144821443	-1.9266758971
H	-2.1563431827	0.2968832386	-1.5502115119
H	-1.4993820997	-2.2772528326	0.3455303013
H	-3.8512944056	0.4119493517	1.3690249772
H	-3.3176394320	-1.2741130684	1.6746594239
H	-4.2915500355	-0.8716910782	0.2701318010

S₀ energy / H -387.80219477126423

S₀ CI eigenvector -0.96804494677227 X36 X37 X38

-0.11184870321220 X36 X37 A38 B39
-0.11184870321220 X36 X37 B38 A39
0.11058939461755 X36 A37 X38 B39
0.11058939461755 X36 B37 X38 A39
0.10190087810522 X36 X38 X39
0.04912619277670 X37 X38 X39

S₁ energy / H -387.80219451298774

S₁ CI eigenvector -0.68943496768376 X36 X37 A38 B39
-0.68943496768376 X36 X37 B38 A39
0.15743063927787 X36 X37 X38
-0.10730489050749 X36 A37 B38 X39
-0.10730489050749 X36 B37 A38 X39

ax-T S₁/S₀ MECl-3 (Open)

Cartesian coordinates / 26
Å

C 0.7600752822 0.2619303598 -0.7345672864
C 0.7830153508 0.2579166972 -2.2720168789
C -0.7406620023 1.6333500825 -0.0491431933
C 0.1707195023 -0.6765232557 0.1320007060
C -0.5335351606 0.1770755693 -3.0511408672
C 1.6153410954 1.4461789347 -2.7729738947
C -1.9938387835 1.0912451088 -0.3986140253
C -2.2399739581 -0.2727143345 -0.1342096149
C -1.1891844003 -1.1166813565 0.1876445025
C -3.6503216637 -0.8011281549 -0.1663487214
H 1.7277392808 0.5751582644 -0.3681904871
H 1.3441360304 -0.6391027403 -2.5394867067

H	-0.4100673102	2.5368989040	-0.5340874852
H	-0.3972326430	1.5559885046	0.9663687377
H	0.7908265143	-0.9891812069	0.9634273798
H	-1.0920788936	1.1032617880	-3.0062249426
H	-0.3070967046	-0.0179020666	-4.0960193106
H	-1.1696708477	-0.6224615044	-2.6958546887
H	1.1271822984	2.3925419434	-2.5577374951
H	1.7612025856	1.3863941928	-3.8472707733
H	2.5974036994	1.4661655867	-2.3099577936
H	-2.6080253153	1.6098152557	-1.1132925299
H	-1.3922595925	-2.0588048690	0.6667396840
H	-4.2051156166	-0.4289940506	0.6899114153
H	-3.6767037322	-1.8840670622	-0.1553257954
H	-4.1651577275	-0.4533539167	-1.0567843432

S_0 energy / H -387.80336467764687

S_0 CI eigenvector

-0.64757822452749	X36	X37	X38
-0.52600073201432	X36	X37	A38 B39
-0.52600073201432	X36	X37	B38 A39
0.08175196382723	X36	X38	X39
0.06172453643308	X37	X38	X39
0.05633790510091	A36	X37	B38 X39
0.05633790510091	B36	X37	A38 X39
-0.05592383401504	X36	A37	B38 X39
-0.05592383401504	X36	B37	A38 X39
-0.03692629107170	X36	X37	X39
0.03170782386289	X36	A37	X38 B39
0.03170782386289	X36	B37	X38 A39

S_1 energy / H -387.80336462500168

S₁ CI eigenvector

0.73768411723328	X36 X37 X38
-0.46159502663600	X36 X37 A38 B39
-0.46159502663600	X36 X37 B38 A39
-0.10233865251497	X37 X38 X39
-0.07053653834627	X36 X38 X39
0.04845815828915	X36 X37 X39
-0.04455288932464	X36 A37 B38 X39
-0.04455288932464	X36 B37 A38 X39
0.03739804278241	A36 X37 X38 B39
0.03739804278241	B36 X37 X38 A39
0.03634317401199	A36 X37 B38 X39
0.03634317401199	B36 X37 A38 X39
-0.02898498174395	X36 A37 X38 B39
-0.02898498174395	X36 B37 X38 A39

ax-T cZc-ZDOT Minimum

Cartesian coordinates / Å	26			
C	1.2262137283	-0.4709174959	-0.7964103447	
C	1.1585813768	-0.7202937895	-2.2886809088	
C	-1.3126608512	2.1604922434	-0.0579900102	
C	0.3182307415	-0.5479889060	0.1640824436	
C	-0.0561263468	-1.4957423448	-2.8020005830	
C	1.3132248648	0.6118619887	-3.0400384177	
C	-2.2381946639	1.2201001551	-0.3434485250	
C	-2.1974653729	-0.2160018617	-0.1001160044	
C	-1.1056778271	-0.9664229034	0.1054498748	
C	-3.5571628023	-0.8844251902	-0.1200457241	
H	2.2107758561	-0.1605178311	-0.4785110005	
H	2.0379107697	-1.3203721912	-2.5212465027	

0.14280142485137 X36 X37 X38
 -0.14148612199564 X36 X38 X39
 -0.03989177177915 A36 X37 X38 B39
 -0.03989177177915 B36 X37 X38 A39
 0.03369976424435 A36 X37 B38 X39
 0.03369976424435 B36 X37 A38 X39
 -0.03126773855448 A36 B37 X38 X39
 -0.03126773855448 B36 A37 X38 X39
 0.02478811920746 X36 A37 B38 X39
 0.02478811920746 X36 B37 A38 X39

ax-G+ - So Minimum (FC)

Cartesian coordinates / 26
Å

C	0.2417848542	0.5701366501	-1.0365749936
C	0.8546216929	0.5714765869	-2.4499952311
C	-1.0090832397	1.4537513061	-0.8627792298
C	-0.2920112659	-0.7461200204	-0.5398810184
C	2.1808000036	-0.1977077169	-2.4771258328
C	-0.0826431040	0.0677752757	-3.5552569029
C	-2.1781085746	0.5188223250	-0.6346404501
C	-2.1199382797	-0.4347732054	0.4079666100
C	-0.8532907428	-0.8537565164	0.7953521084
C	-3.3812709159	-1.1001204819	0.8962881300
H	1.0153605740	0.8752799282	-0.3319253066
H	1.0813164136	1.6136136112	-2.6683074401
H	-1.1714313208	2.0607451758	-1.7457945641
H	-0.8916230957	2.1390167356	-0.0229087410

H -0.2254846849 -1.6212861413 -1.1698089689
H 2.0374899805 -1.2525863255 -2.2564921360
H 2.6464459493 -0.1333569981 -3.4557466112
H 2.8820119421 0.1992920618 -1.7493746399
H -0.2891439292 -0.9936089832 -3.4589723916
H 0.3777200529 0.2202927156 -4.5269592696
H -1.0338969041 0.5871290276 -3.5552808382
H -3.1318636476 0.7526938900 -1.0752606424
H -0.7413589069 -1.7518304230 1.3744045335
H -3.6474338275 -1.9240059857 0.2409085387
H -4.2099822650 -0.3998897440 0.9083994734
H -3.2353313542 -1.4981302333 1.8930299388

S₀ energy / H -387.80663156815126

S₀ CI eigenvector -0.58318663210468 X36 X37 A38 B39
-0.58318663210468 X36 X37 B38 A39
0.53343576501733 X36 X37 X38
0.11705072203375 X36 A37 B38 X39
0.11705072203375 X36 B37 A38 X39
-0.06118923433112 X36 X38 X39
0.04007527920139 X36 A37 X38 B39
0.04007527920139 X36 B37 X38 A39
-0.02315067218226 X37 X38 X39

S₁ energy / H -387.80663149768958

S₁ CI eigenvector -0.82259159908024 X36 X37 X38
-0.37505867221203 X36 X37 A38 B39
-0.37505867221203 X36 X37 B38 A39
-0.10593731455118 X36 A37 X38 B39
-0.10593731455118 X36 B37 X38 A39
0.09019604216599 X36 X38 X39

0.06967442377067 X36 A37 B38 X39

0.06967442377067 X36 B37 A38 X39

0.03529369718816 X37 X38 X39

Ax-G+ - S₁/S₀ MECI-1 (Closed)

Cartesian coordinates / 26

Å

C	0.1979337252	0.7696784185	-1.1184560652
C	0.8099382383	0.4867837568	-2.5228037267
C	-1.2188185788	1.4210002335	-1.1895952109
C	0.2273857230	-0.4638820890	-0.2442485828
C	2.2944929198	0.1069655953	-2.4482692050
C	0.0329359314	-0.5417071924	-3.3524142698
C	-2.4336022205	0.5062040787	-0.8860299446
C	-2.1499743709	-0.4242483781	0.1376037291
C	-0.8353938360	-1.0739851565	0.2811295533
C	-3.2108939813	-0.8400664046	1.1122189883
H	0.8883631806	1.4749939816	-0.6557015851
H	0.7561913661	1.4380405851	-3.0464531356
H	-1.3497493330	1.8761058939	-2.1639416020
H	-1.2580989772	2.2400051051	-0.4773086444
H	1.1998972685	-0.8773652419	-0.0332719152
H	2.4459171497	-0.8829197728	-2.0272304194
H	2.7316716465	0.1016806575	-3.4419085203
H	2.8562318881	0.8158005489	-1.8464054960
H	-0.0056265028	-1.5070761617	-2.8549374287
H	0.5168976240	-0.6914094896	-4.3130089066
H	-0.9835836627	-0.2211635455	-3.5469311405
H	-2.1353904445	-0.3620779845	-1.5719062675
H	-0.7155419682	-1.9346002339	0.9172099065

H -3.8297808318 0.0191453440 1.3348112218
H -2.8106144869 -1.2922825550 2.0139165426
H -3.8476339188 -1.5721954203 0.6218562600

S₀ energy / H -387.80181805115842

S₀ CI eigenvector -0.64799097481248 X36 X37 A38 B39
-0.64799097481248 X36 X37 B38 A39
0.36632801375322 X36 X37 X38
-0.10099624051597 X36 A37 B38 X39
-0.10099624051597 X36 B37 A38 X39
-0.03812499714040 X36 A37 X38 B39
-0.03812499714040 X36 B37 X38 A39
-0.03558014074478 X36 X38 X39
-0.02337175802583 X37 X38 X39

S₁ energy / H -387.80181795300194

S₁ CI eigenvector 0.90973354915533 X36 X37 X38
0.26066575682312 X36 X37 A38 B39
0.26066575682312 X36 X37 B38 A39
-0.10502402148164 X36 A37 X38 B39
-0.10502402148164 X36 B37 X38 A39
-0.09587225581004 X36 X38 X39
-0.04583590102241 X37 X38 X39
0.03757149430946 X36 A37 B38 X39
0.03757149430946 X36 B37 A38 X39

Ax-G+ - S₁/S₀ MECI-2 (Closed)

Cartesian coordinates / 26
Å

C 0.1979337252 0.7696784185 -1.1184560652
C 0.8099382383 0.4867837568 -2.5228037267

C	-1.2188185788	1.4210002335	-1.1895952109
C	0.2273857230	-0.4638820890	-0.2442485828
C	2.2944929198	0.1069655953	-2.4482692050
C	0.0329359314	-0.5417071924	-3.3524142698
C	-2.4336022205	0.5062040787	-0.8860299446
C	-2.1499743709	-0.4242483781	0.1376037291
C	-0.8353938360	-1.0739851565	0.2811295533
C	-3.2108939813	-0.8400664046	1.1122189883
H	0.8883631806	1.4749939816	-0.6557015851
H	0.7561913661	1.4380405851	-3.0464531356
H	-1.3497493330	1.8761058939	-2.1639416020
H	-1.2580989772	2.2400051051	-0.4773086444
H	1.1998972685	-0.8773652419	-0.0332719152
H	2.4459171497	-0.8829197728	-2.0272304194
H	2.7316716465	0.1016806575	-3.4419085203
H	2.8562318881	0.8158005489	-1.8464054960
H	-0.0056265028	-1.5070761617	-2.8549374287
H	0.5168976240	-0.6914094896	-4.3130089066
H	-0.9835836627	-0.2211635455	-3.5469311405
H	-2.1353904445	-0.3620779845	-1.5719062675
H	-0.7155419682	-1.9346002339	0.9172099065
H	-3.8297808318	0.0191453440	1.3348112218
H	-2.8106144869	-1.2922825550	2.0139165426
H	-3.8476339188	-1.5721954203	0.6218562600

So energy / H -387.80181805115842

So CI eigenvector -0.64799097481248 X36 X37 A38 B39

-0.64799097481248 X36 X37 B38 A39

0.36632801375322 X36 X37 X38

-0.10099624051597 X36 A37 B38 X39

	-0.10099624051597 X36 B37 A38 X39
	-0.03812499714040 X36 A37 X38 B39
	-0.03812499714040 X36 B37 X38 A39
	-0.03558014074478 X36 X38 X39
	-0.02337175802583 X37 X38 X39
S ₁ energy / H	-387.80181795300194
S ₁ CI eigenvector	0.90973354915533 X36 X37 X38
	0.26066575682312 X36 X37 A38 B39
	0.26066575682312 X36 X37 B38 A39
	-0.10502402148164 X36 A37 X38 B39
	-0.10502402148164 X36 B37 X38 A39
	-0.09587225581004 X36 X38 X39
	-0.04583590102241 X37 X38 X39
	0.03757149430946 X36 A37 B38 X39
	0.03757149430946 X36 B37 A38 X3

Ax-G+ - S₁/S₀ MECI-3 (Open)

Cartesian coordinates / Å	26		
C	0.7287161387	0.2030187308	-0.8467286336
C	0.6470982265	0.2015435846	-2.3786516980
C	-0.6802286569	1.5984392577	-0.0854244165
C	0.1821062931	-0.7173309423	0.0597495139
C	1.7227340677	-0.7705250334	-2.8997429549
C	-0.6822165347	-0.1306513745	-3.0620960643
C	-1.9711535468	1.0945290671	-0.3590505622
C	-2.2255840353	-0.2713006541	-0.1132311535
C	-1.1823834620	-1.1409658490	0.1586514114
C	-3.6416280126	-0.7829545171	-0.1295145312
H	1.7133214126	0.5342864678	-0.5464606234
H	0.9366131510	1.2003190121	-2.7016356517

H	-0.3452279821	2.4832470546	-0.6035924735
H	-0.2859495416	1.5302793727	0.9130282360
H	0.8322570126	-1.0169782959	0.8729685086
H	1.4641387215	-1.7927249911	-2.6375792745
H	1.8026831650	-0.7110449861	-3.9818652319
H	2.7006528636	-0.5566226713	-2.4802207014
H	-1.0652241982	-1.0945575777	-2.7496025960
H	-0.5194412703	-0.1702249153	-4.1356342580
H	-1.4398831915	0.6138642010	-2.8720042665
H	-2.6104205837	1.6355815820	-1.0341993391
H	-1.3860072978	-2.0946448203	0.6136039693
H	-4.1764615510	-0.4397433846	0.7508253112
H	-3.6751287676	-1.8651913987	-0.1608918579
H	-4.1693448474	-0.3969120278	-0.9961449871

So energy / H -387.80483862897137

So CI eigenvector -0.95975759923633 X36 X37 X38
-0.14781598943905 X36 X37 A38 B39
-0.14781598943905 X36 X37 B38 A39
0.11114463245535 X37 X38 X39
0.10508230583397 X36 X38 X39
-0.05190930957953 X36 X37 X39
0.04650013862945 X36 A37 X38 B39
0.04650013862945 X36 B37 X38 A39
-0.02803180795458 A36 B37 X38 X39
-0.02803180795458 B36 A37 X38 X39
-0.02531857949088 A36 X37 X38 B39
-0.02531857949088 B36 X37 X38 A39
0.02438265916908 A36 X37 B38 X39
0.02438265916908 B36 X37 A38 X39

S ₁ energy / H	-387.80483844324084
S ₁ CI eigenvector	-0.68375200325077 X36 X37 A38 B39
	-0.68375200325077 X36 X37 B38 A39
	0.20754459505639 X36 X37 X38
	-0.07332504654601 X36 A37 B38 X39
	-0.07332504654601 X36 B37 A38 X39
	0.06002297019828 A36 X37 B38 X39
	0.06002297019828 B36 X37 A38 X39
	-0.04455957191723 X37 X38 X39
	0.02801839030162 A36 X37 X38 B39
	0.02801839030162 B36 X37 X38 A3

Ax-G+ cZc-ZDOT Minimum

Cartesian coordinates / Å	26
C	1.2167540946 -0.4263481655 -0.8569819289
C	1.1402182129 -0.6871393715 -2.3472869257
C	-1.3497894335 2.1558913897 -0.0846773421
C	0.3260912437 -0.5193955953 0.1185604699
C	2.3580028781 -1.5247600642 -2.7688914272
C	-0.1492815735 -1.3292490863 -2.8614041022
C	-2.2875347749 1.2022024154 -0.2677975836
C	-2.2046778391 -0.2343365681 -0.0422410692
C	-1.0901570403 -0.9671671327 0.0976530589
C	-3.5501090893 -0.9300777802 0.0010500629
H	2.2000225813 -0.1019978867 -0.5497176457
H	1.2362961754 0.2857772751 -2.8299142516
H	-1.5838347448 3.1837912708 -0.2947945179
H	-0.3609873960 1.9491448650 0.2707039006

H 0.6874805475 -0.2778796620 1.1091982699
H 2.3282822282 -2.5077366650 -2.3071481271
H 2.3786983156 -1.6607554925 -3.8456788845
H 3.2893071565 -1.0485454934 -2.4773758954
H -0.3328087981 -2.2867461875 -2.3840971873
H -0.0679507446 -1.5036173543 -3.9304102188
H -1.0101961004 -0.6975264821 -2.6904588913
H -3.2579232981 1.5403941351 -0.5961475093
H -1.2230583946 -2.0206418042 0.2881621825
H -4.1769896962 -0.5126956589 0.7845108326
H -3.4486583050 -1.9931495903 0.1804553947
H -4.0825162054 -0.7973653108 -0.9376006641

S₀ energy / H -387.91686946030802

S₀ CI eigenvector -0.96934101487212 X36 X37 X38
0.11972552996098 X36 X37 X39
-0.11476083098522 X36 X37 A38 B39
-0.11476083098522 X36 X37 B38 A39
0.09461400324175 X36 X38 X39
0.06827796568446 X36 A37 B38 X39
0.06827796568446 X36 B37 A38 X39

S₁ energy / H -387.7188817407411

S₁ CI eigenvector 0.63712461440479 X36 X37 A38 B39
0.63712461440479 X36 X37 B38 A39
-0.22171951676535 X36 A37 X38 B39
-0.22171951676535 X36 B37 X38 A39
-0.19783083056383 X36 X37 X39
-0.14841740420460 X36 X37 X38
0.14788885665153 X36 X38 X39

0.03408096242917 A36 X37 X38 B39
0.03408096242917 B36 X37 X38 A39
-0.02928668817313 A36 X37 B38 X39
-0.02928668817313 B36 X37 A38 X39
-0.02661533151651 A36 B37 X38 X39
-0.02661533151651 B36 A37 X38 X39
0.02579770266313 X36 A37 B38 X39
0.02579770266313 X36 B37 A38 X39

eq-G- S₀ Minimum (FC)

Cartesian coordinates / 26
Å

C	0.7215842185	-0.0176476731	0.1956837804
C	2.1871475914	-0.0476244843	-0.2973649979
C	-0.0231118548	1.2737258499	-0.1832592245
C	-0.0785385643	-1.2088974162	-0.2865091147
C	2.9437810903	1.2482435975	0.0212230012
C	2.9593750992	-1.2324084311	0.2987129588
C	-1.5046217313	1.1881932906	0.0822919164
C	-2.1705195596	0.0346739532	-0.0151504071
C	-1.4270730878	-1.1696272090	-0.3448711194
C	-3.6615937916	-0.0703838162	0.1758983077
H	0.7459488470	-0.0627673021	1.2883797787
H	2.1685409125	-0.1643166350	-1.3802441370
H	0.1314014948	1.4797909357	-1.2453625462
H	0.3920133693	2.1165617483	0.3563176005
H	0.4328696946	-2.1208024234	-0.5332548962
H	2.9163864131	1.4643798018	1.0867630772
H	3.9864562843	1.1578140542	-0.2675142581

H 2.5366999143 2.1042667572 -0.5037653823
H 3.0311326718 -1.1384796418 1.3793814673
H 3.9700914053 -1.2659107955 -0.0963739498
H 2.4969600581 -2.1882085833 0.0825018220
H -2.0292503802 2.1024847742 0.3029085326
H -1.9777469460 -2.0500451328 -0.6305709975
H -4.1021050295 0.8942966314 0.3986780990
H -3.9038770024 -0.7495828821 0.9891074074
H -4.1393511169 -0.4605289679 -0.719406718

S₀ energy / H

S₀ CI eigenvector

-387.96100444601700
-0.97519068229222 X36 X37 X38
0.11632710709177 X36 X37 X39
0.09633384418636 X36 X37 A38 B39
0.09633384418636 X36 X37 B38 A39
0.08682545112113 X36 X38 X39
-0.05806737301177 X36 A37 B38 X39
-0.05806737301177 X36 B37 A38 X39
0.03061420004001 A36 X37 B38 X39
0.03061420004001 B36 X37 A38 X39

S₁ energy / H

S₁ CI eigenvector

-387.77243518781489
-0.66680452344343 X36 X37 A38 B39
-0.66680452344343 X36 X37 B38 A39
-0.16384811375325 X36 A37 X38 B39
-0.16384811375325 X36 B37 X38 A39
-0.14076336339304 X36 X37 X39
-0.13290784952594 X36 X37 X38
0.09926063151556 X36 X38 X39
-0.04867673559357 X36 A37 B38 X39

-0.04867673559357 X36 B37 A38 X39
-0.03474854513125 A36 X37 B38 X39
-0.03474854513125 B36 X37 A38 X39
0.03145485319226 A36 X37 X38 B39
0.03145485319226 B36 X37 X38 A39

eq-G- S₁/S₀ MECI-1 (Closed)

Cartesian coordinates / 26
Å

C	0.8205846739	0.2056237093	0.5701030249
C	2.0239412939	0.0476758007	-0.3772567085
C	-0.0491291391	1.4578870690	0.3775027571
C	-0.2250101521	-0.8674528447	0.3842313533
C	3.0040730779	1.2122506109	-0.2100399871
C	2.7322354646	-1.2939719954	-0.1578851361
C	-1.4760188018	1.0100455143	0.6203765233
C	-2.0257626551	0.0051221609	-0.2086215388
C	-1.1090933929	-0.8737839235	-0.7721684666
C	-3.5166093311	-0.2054856091	-0.2836208056
H	1.1706646381	0.1724767687	1.5994590956
H	1.6364802501	0.0646366178	-1.3919447569
H	0.0476778765	1.8443099289	-0.6371753129
H	0.2377228012	2.2495221910	1.0592224010
H	-0.2962895087	-1.6526282735	1.1242266122
H	3.4024449218	1.2467612720	0.8011088545
H	3.8430192727	1.1104875417	-0.8919962212
H	2.5316097121	2.1673471756	-0.4132297416
H	3.0949339780	-1.3856679017	0.8633568841
H	3.5861915268	-1.3958827963	-0.8205842000

H 2.0701805684 -2.1329565228 -0.3525684046
H -2.1230498577 1.5944887338 1.2504867304
H -1.4321210927 -1.7893763946 -1.2317389901
H -4.0564177275 0.7185871082 -0.1070306019
H -3.8322956727 -0.9320161742 0.4593472024
H -3.7848547101 -0.5927407573 -1.2599603127

S₀ energy / H -387.80956229542915

S₀ CI eigenvector 0.58512611242490 X36 X37 X38
-0.55711001454199 X36 X37 A38 B39
-0.55711001454199 X36 X37 B38 A39
0.11460965090409 X36 A37 B38 X39
0.11460965090409 X36 B37 A38 X39
-0.06988733178561 X36 X38 X39
0.04865608199524 X36 A37 X38 B39
0.04865608199524 X36 B37 X38 A39
-0.02509910410607 X37 X38 X39

S₁ energy / H -387.80956226639279

S₁ CI eigenvector -0.78540814846225 X36 X37 X38
-0.41198449833168 X36 X37 A38 B39
-0.41198449833168 X36 X37 B38 A39
-0.10461145972005 X36 A37 X38 B39
-0.10461145972005 X36 B37 X38 A39
0.08889472040544 X36 X38 X39
0.07822105820126 X36 A37 B38 X39
0.07822105820126 X36 B37 A38 X39
0.03351048927819 X37 X38 X39

eq-G- S₁/S₀ MECI-2 (Closed)

Cartesian coordinates / 26
Å

C	0.7724558188	0.0881489672	0.2575458415
C	2.1641725098	-0.0301612690	-0.4149372244
C	-0.0953169535	1.2859829156	-0.2199619392
C	0.0013187188	-1.2022528236	0.1664981594
C	2.8643924751	1.3301594762	-0.5178322918
C	3.0899203241	-1.0125060859	0.3162115250
C	-1.5893856116	1.2244938718	0.2010323763
C	-2.1032783329	-0.0733967160	-0.0479152003
C	-1.3347114484	-1.2994743567	0.1253622107
C	-3.5198039553	-0.2291249812	-0.5082117168
H	0.9334500337	0.2393880853	1.3310635797
H	2.0086792564	-0.3982033194	-1.4288842151
H	-0.0528859469	1.3526859865	-1.3066551869
H	0.3385638732	2.2015648128	0.1573238533
H	0.5648228322	-2.1195474218	0.1592786458
H	2.3133401099	2.0305406558	-1.1321480463
H	2.9925329792	1.7761990325	0.4652017450
H	3.8500695782	1.2125511006	-0.9572133342
H	3.2938458834	-0.6673817568	1.3264566539
H	4.0407637876	-1.0957321960	-0.2006340527
H	2.6799381386	-2.0142489723	0.3880038954
H	-1.4044340302	0.8469200358	1.2705441974
H	-1.8086803251	-2.2636121218	0.0569376242
H	-4.1630174545	0.0337230138	0.3259636754
H	-3.7733680767	-1.2266639856	-0.8496290174
H	-3.6979371855	0.5169857453	-1.2733276221

S₀ energy / H -387.80592223014224
 S₀ CI eigenvector 0.69616470434947 X36 X37 A38 B39
 0.69616470434947 X36 X37 B38 A39
 0.09227620068639 X36 X37 X38
 -0.08860596014356 A36 X37 B38 X39
 -0.08860596014356 B36 X37 A38 X39
 -0.05353036383453 X36 A37 B38 X39
 -0.05353036383453 X36 B37 A38 X39

S₁ energy / H -387.80592209503504
 S₁ CI eigenvector -0.97776450793694 X36 X37 X38
 0.08651795125359 X37 X38 X39
 -0.08511072749567 X36 A37 X38 B39
 -0.08511072749567 X36 B37 X38 A39
 0.06703208733617 X36 X38 X39
 0.06576866316932 X36 X37 A38 B39
 0.06576866316932 X36 X37 B38 A39
 -0.06375019652245 A36 X37 X38 B39
 -0.06375019652245 B36 X37 X38 A39

eq-G- S₁/S₀ MECI-3 (Open)

Cartesian coordinates / 26
 Å
 C 0.8645538360 -0.0952671421 0.0089172085
 C 2.3611565855 -0.2204773165 -0.2170248598
 C -0.4798137648 1.6344741216 -0.6225996939
 C -0.0263071444 -0.9367252573 -0.6613854982
 C 3.0818100555 1.0908440900 0.1151330204
 C 2.9729992878 -1.3780238197 0.5920812997
 C -1.6489315323 1.3311922368 0.1035809977

C	-2.1940256412	0.0547380452	-0.0246396753
C	-1.4364637360	-0.9692238870	-0.6222635145
C	-3.5818141064	-0.2367650660	0.4785190911
H	0.5757732206	0.2918034307	0.9704747946
H	2.5348859884	-0.4326971590	-1.2710366892
H	-0.4065519467	1.3349330604	-1.6502217991
H	0.1155975129	2.4877297847	-0.3504589850
H	0.4226522944	-1.6489164584	-1.3425565291
H	2.8964228245	1.3804213742	1.1467215403
H	4.1564963508	0.9939998763	-0.0104347429
H	2.7429862726	1.9010520633	-0.5229560802
H	2.8173893362	-1.2293701922	1.6572890695
H	4.0439384611	-1.4575138773	0.4188288234
H	2.5205059167	-2.3274785958	0.3227543418
H	-2.0049691761	2.0113206899	0.8566727426
H	-1.9360179036	-1.8325148995	-1.0244789700
H	-4.0772366140	0.6582876061	0.8338679088
H	-3.5503935388	-0.9690005425	1.2793224344
H	-4.1784777464	-0.6631974590	-0.3227357354

So energy / H -387.82385202031855

So CI eigenvector -0.69350859306081 X36 X37 A38 B39
 -0.69350859306081 X36 X37 B38 A39
 0.13019679049011 X36 X37 X38
 -0.09760916431948 X36 A37 B38 X39
 -0.09760916431948 X36 B37 A38 X39
 -0.03104039399901 X36 X38 X39
 0.02315939544216 X36 X37 X3

S1 energy / H -387.82385189660880

S₁ CI eigenvector

0.97107198284765 X36 X37 X38

-0.14405395540441 X36 X38 X39

0.09587170452449 X36 X37 A38 B39

0.09587170452449 X36 X37 B38 A39

-0.08012434328866 X37 X38 X39

0.06549146721486 X36 X37 X39

-0.05782472008042 X36 A37 X38 B39

-0.05782472008042 X36 B37 X38 A39

eq-G- cZc-EDOT Minimum

Cartesian coordinates / 26
 Å

C	1.1304329602	-0.6808460378	0.1531111476
C	2.6108857186	-0.8726431806	-0.0582562878
C	-0.8397391593	2.1781603942	-0.3330961895
C	0.1826872384	-1.1238807229	-0.6662253754
C	3.3168251808	0.4797027822	-0.2296180574
C	3.2280019423	-1.6642512586	1.1027154228
C	-1.5180011267	1.3362282260	0.4263986706
C	-2.0141919731	0.0035058644	0.0151788084
C	-1.2671213438	-0.9977242344	-0.5134790172
C	-3.5047389718	-0.1731498095	0.2036390696
H	0.8513437450	-0.1391939872	1.0426050131
H	2.7529239070	-1.4449278437	-0.9718693548
H	-0.5348543828	1.9197469593	-1.3310549044
H	-0.5581763229	3.1524309024	0.0257170257
H	0.4921310612	-1.7089542178	-1.5203398084
H	3.1929135743	1.0984489536	0.6553718593
H	4.3822420307	0.3430806567	-0.3911941615
H	2.9144137370	1.0254576344	-1.0767109078

H 3.1046789773 -1.1340957527 2.0435838755
H 4.2918904388 -1.8178571709 0.9460700741
H 2.7577650806 -2.6366969437 1.2048889576
H -1.8250750906 1.6676335611 1.4084721413
H -1.8128539633 -1.8591925958 -0.8652825050
H -3.7805972017 -0.0713139520 1.2518827207
H -3.8350880037 -1.1493028144 -0.1308188385
H -4.0639280527 0.5824345881 -0.3433293788

S₀ energy / H -387.92638919143826

S₀ CI eigenvector 0.98729585419654 X36 X37 X38
-0.09333196538926 X36 X37 X39
-0.07379587045791 X37 X38 X39
-0.05689852958353 A36 X37 B38 X39
-0.05689852958353 B36 X37 A38 X39
0.03806106086014 X36 X37 A38 B39
0.03806106086014 X36 X37 B38 A39
-0.03748386015648 X36 X38 X39

S₁ energy / H -387.73789017951913

S₁ CI eigenvector 0.68854109167997 X36 X37 A38 B39
0.68854109167997 X36 X37 B38 A39
-0.11757409596283 A36 X37 X38 B39
-0.11757409596283 B36 X37 X38 A39
-0.09020469298112 X36 A37 B38 X39
-0.09020469298112 X36 B37 A38 X39
-0.05276435889037 X36 X37 X38
-0.05123689289574 X36 X37 X39
0.03517039062917 X37 X38 X39
0.02328033685207 X36 A37 X38 B39

eq-T So Minimum (FC)

Cartesian coordinates / 26
Å

C	0.7057597469	0.0237544854	0.1411151022
C	2.1723001798	-0.0213651958	-0.3431453567
C	-0.1260218952	1.1862578378	-0.4248841664
C	-0.0132019614	-1.2857727150	-0.0859510646
C	2.3222236753	-0.2396929353	-1.8536175369
C	2.9686119337	1.2090630395	0.1040870397
C	-1.5944317799	1.0447811606	-0.1112177847
C	-2.1788127838	-0.1508849697	0.0088839364
C	-1.3617565860	-1.3479548047	-0.1079293012
C	-3.6580792044	-0.3159238124	0.2468169455
H	0.7446689661	0.1675857197	1.2242459065
H	2.6172269885	-0.8844624529	0.1506684005
H	-0.0140835236	1.2329888968	-1.5085834025
H	0.2422429672	2.1306146352	-0.0390170489
H	0.5697536686	-2.1895358151	-0.1363372372
H	1.9850938788	0.6221323403	-2.4208210383
H	3.3653477121	-0.4044559118	-2.1072800077
H	1.7583117501	-1.1011605270	-2.1955237782
H	2.6314201107	2.1106839297	-0.3982812198
H	4.0228904957	1.0862604543	-0.1254590171
H	2.8800568115	1.3709888251	1.1745859597
H	-2.1823613767	1.9447068789	-0.0466656314
H	-1.8567961662	-2.3008172372	-0.1900486800
H	-4.1601928511	0.6425655125	0.3052079878
H	-3.8468681307	-0.8537281379	1.1723299508

H -4.1173026260 -0.8886292005 -0.5551789576

S₀ energy / H -387.96159429897074
S₀ CI eigenvector -0.97493281468196 X36 X37 X38
0.11662336390680 X36 X37 X39
-0.09735180221812 X36 X37 A38 B39
-0.09735180221812 X36 X37 B38 A39
0.08655202046549 X36 X38 X39
-0.05799785652372 X36 A37 B38 X39
-0.05799785652372 X36 B37 A38 X39
0.03116916936685 A36 X37 B38 X39
0.03116916936685 B36 X37 A38 X39

S₁ energy / H -387.77315039506851
S₁ CI eigenvector -0.66640928234247 X36 X37 A38 B39
-0.66640928234247 X36 X37 B38 A39
-0.16438042434047 X36 A37 X38 B39
-0.16438042434047 X36 B37 X38 A39
0.14207072500754 X36 X37 X39
0.13453150546971 X36 X37 X38
-0.09879323528164 X36 X38 X39
0.04850522885015 X36 A37 B38 X39
0.04850522885015 X36 B37 A38 X39
0.03455292093703 A36 X37 B38 X39
0.03455292093703 B36 X37 A38 X39
0.03128328492401 A36 X37 X38 B39
0.03128328492401 B36 X37 X38 A39

Cartesian coordinates / 26

Å

C	0.7607767557	0.2409503832	0.4054968458
C	2.0450281606	0.0504225558	-0.4355621621
C	-0.1295918459	1.4669736053	0.1750342942
C	-0.2731490417	-0.8573214356	0.2861859717
C	1.8248738289	-0.1023877659	-1.9450035070
C	3.0280385578	1.1923050715	-0.1487110497
C	-1.5103882391	1.0098828195	0.5972806452
C	-2.1354034838	-0.0274553305	-0.1450278911
C	-1.2713280193	-0.9073077576	-0.7732287345
C	-3.6219740359	-0.2476692916	-0.0459023764
H	1.0697267814	0.2605708474	1.4475878802
H	2.5075801987	-0.8706427150	-0.0804400936
H	-0.1415200431	1.7610378429	-0.8734459666
H	0.2026411342	2.3188512508	0.7556178151
H	-0.2311649265	-1.6637149295	1.0069039108
H	1.4002192874	0.7941514475	-2.3834803788
H	2.7769793192	-0.2892192569	-2.4347360761
H	1.1585288062	-0.9224551794	-2.1769922009
H	2.6359064585	2.1441293527	-0.4952392475
H	3.9721958077	1.0227971808	-0.6575899357
H	3.2359829075	1.2846150026	0.9134345938
H	-2.0917254058	1.5943327642	1.2881794798
H	-1.6186748439	-1.8383577149	-1.1799877587
H	-4.1467999680	0.6964766869	0.0560510525
H	-3.8486061015	-0.8545250142	0.8257667908
H	-3.9883817482	-0.7698450793	-0.9217480950

So energy / H -387.80500974883802

So CI eigenvector 0.97192763752711 X36 X37 X38

-0.11745472841741 X36 X38 X39
 0.11160470710375 X36 A37 X38 B39
 0.11160470710375 X36 B37 X38 A39
 -0.08250169116511 X36 X37 A38 B39
 -0.08250169116511 X36 X37 B38 A39
 -0.04076355267413 X37 X38 X39
 -0.02371222048129 X36 X37 X39

S₁ energy / H -387.80500962784629
 S₁ CI eigenvector 0.68762268207827 X36 X37 A38 B39
 0.68762268207827 X36 X37 B38 A39
 -0.13985120101163 X36 A37 B38 X39
 -0.13985120101163 X36 B37 A38 X39
 0.11400361728325 X36 X37 X38
 0.02961637043922 X36 A37 X38 B39
 0.02961637043922 X36 B37 X38 A39

eq-T S₁/S₀ MECI-2 (Closed)

Cartesian coordinates / 26
 Å

C 0.7687321046 0.1112457476 0.2414067123
 C 2.1687557267 -0.0107788136 -0.4069880475
 C -0.1656619577 1.2190177012 -0.3188610698
 C 0.0825120003 -1.2247692879 0.3026601893
 C 2.1141315226 -0.4418339439 -1.8783183976
 C 2.9729331498 1.2830718783 -0.2526130910
 C -1.6540457600 1.0944556487 0.1131239454
 C -2.0843954276 -0.2534453343 0.0020587929
 C -1.2441465497 -1.4075437311 0.2982265965
 C -3.4898173244 -0.5468893562 -0.4238838795

H	0.9296824607	0.3662585649	1.2947943040
H	2.7022737959	-0.7884113381	0.1406966856
H	-0.1334649623	1.2237338250	-1.4053593580
H	0.2128612604	2.1813995400	-0.0011049598
H	0.7176552703	-2.0920771836	0.3975985709
H	1.5724124368	-1.3745768407	-2.0098686396
H	1.6313701980	0.3074606847	-2.4959843021
H	3.1163741752	-0.5900020278	-2.2686048355
H	2.5428846835	2.0901155110	-0.8358716046
H	3.9942066581	1.1414730802	-0.5925145718
H	3.0107000051	1.6047814284	0.7840649706
H	-1.4455860259	0.8419909603	1.2144988436
H	-1.6622656444	-2.3977957067	0.3508660194
H	-4.1465833977	-0.2225633692	0.3767652152
H	-3.6833151334	-1.5921435157	-0.6391440536
H	-3.7124993752	0.0873558888	-1.2737004909

S₀ energy / H -387.80720210961749

S₀ CI eigenvector

-0.63870299452758	X36	X37	A38	B39
-0.63870299452758	X36	X37	B38	A39
0.39972856902206	X36	X37	X38	
0.07399792765471	A36	X37	B38	X39
0.07399792765471	B36	X37	A38	X39
-0.06172236205932	X36	A37	B38	X39
-0.06172236205932	X36	B37	A38	X39
-0.04076503536987	X36	A37	X38	B39
-0.04076503536987	X36	B37	X38	A39
-0.03600000405787	X37	X38	X39	
-0.02968698031213	X36	X38	X3	

S₁ energy / H -387.80720201363135

S₁ CI eigenvector

-0.89703060374286 X36 X37 X38

-0.28448203187155 X36 X37 A38 B39

-0.28448203187155 X36 X37 B38 A39

0.08348704968869 X36 A37 X38 B39

0.08348704968869 X36 B37 X38 A39

0.07374053821242 X37 X38 X39

0.06548869326992 X36 X38 X39

-0.05383556111760 A36 X37 X38 B39

-0.05383556111760 B36 X37 X38 A39

0.03341790728550 A36 X37 B38 X39

0.03341790728550 B36 X37 A38 X39

-0.02359527063297 X36 A37 B38 X39

eq-T S₁/S₀ MECI-3 (Open)

Cartesian coordinates /
Å

26

C 0.9095339727 -0.0484331258 -0.0145314402

C 2.4043536677 -0.0444539669 -0.3004398358

C -0.6140307484 1.2605330511 -1.0733290568

C 0.1142566625 -1.1501561702 -0.3416282763

C 2.7170111627 -0.1369487777 -1.8004323764

C 3.0597019168 1.2034339509 0.2990071460

C -1.7322649527 1.0753231098 -0.2360560362

C -2.1417125342 -0.2268026002 0.0502701397

C -1.2831609853 -1.3065251392 -0.2228198041

C -3.5149561917 -0.4695766576 0.6178650859

H 0.5862682481 0.5806494983 0.7942841497

H 2.8691181041 -0.9107573943 0.1781022715

H -0.5162613603 0.6694718828 -1.9631322573

H	-0.1166549753	2.2136853439	-1.1021302435
H	0.6281030632	-1.9970853961	-0.7783569712
H	2.3174378144	0.7237250566	-2.3298834921
H	3.7889243003	-0.1693223792	-1.9758097948
H	2.2879820292	-1.0284835047	-2.2474674697
H	2.6433039812	2.1096171065	-0.1342353788
H	4.1298929343	1.2109819630	0.1157456207
H	2.9071979689	1.2498611373	1.3730552513
H	-2.1539588949	1.9137546092	0.2885955467
H	-1.6910535089	-2.2986023907	-0.3061337975
H	-4.2145320376	-0.6366491780	-0.1976406605
H	-3.8650939060	0.3925009507	1.1739962064
H	-3.5360107075	-1.3399039953	1.2622727925

So energy / H -387.82229947872599

So CI eigenvector

0.58775178793951	X36 X37 A38 B39
0.58775178793951	X36 X37 B38 A39
0.53104751369019	X36 X37 X38
-0.09031680732821	X36 X38 X39
-0.07797737688523	X36 A37 B38 X39
-0.07797737688523	X36 B37 A38 X39
0.05596380898023	X36 X37 X39
-0.04928821467268	X37 X38 X39
0.02206405608562	X36 A37 X38 B39
0.02206405608562	X36 B37 X38 A39

S₁ energy / H -387.82229908597662

S₁ CI eigenvector

-0.82271966075544	X36 X37 X38
0.38303160573690	X36 X37 A38 B39
0.38303160573690	X36 X37 B38 A39

0.11641835123835 X36 X38 X39
0.07026407790796 X37 X38 X39
-0.06080567079592 X36 X37 X39
-0.04515824235417 X36 A37 X38 B39
-0.04515824235417 X36 B37 X38 A39
-0.03874787926089 X36 A37 B38 X39
-0.03874787926089 X36 B37 A38 X3

eq-T cZc-EDOT Minimum

Cartesian coordinates / 26

Å

C	1.0962937617	-0.7437084803	0.1187906338
C	2.5784273855	-0.9430739121	-0.1005682561
C	-0.8491385437	2.0587091358	-0.7375281197
C	0.0999406563	-1.2777773747	-0.5793084452
C	2.9316018990	-1.9482684154	-1.1973467000
C	3.2538553380	0.4118305896	-0.3650625402
C	-1.4801362514	1.3720170901	0.1984734119
C	-2.0269544013	0.0042657496	0.0506468334
C	-1.3343727055	-1.0914261003	-0.3493704851
C	-3.5024156684	-0.0977276454	0.3684862025
H	0.8541511774	-0.0843802515	0.9359452259
H	2.9846312340	-1.3238424698	0.8368144877
H	-0.6298542426	1.6325425825	-1.6998220723
H	-0.5221819891	3.0691135703	-0.5659913635
H	0.3339182122	-1.9804019920	-1.3627237568
H	2.5764377184	-1.6159904974	-2.1683545036
H	4.0086103012	-2.0668852925	-1.2634683732
H	2.5030384298	-2.9246786351	-0.9971472383
H	2.9066016755	0.8382236794	-1.3016790344

H 4.3326280947 0.3018702704 -0.4238711746
H 3.0349166896 1.1233115206 0.4253637654
H -1.7000717027 1.8659234599 1.1346346124
H -1.9162051507 -1.9856578828 -0.5103255262
H -3.7008369536 0.1864134829 1.4005579276
H -3.8705728381 -1.1070557719 0.2280202815
H -4.0883221262 0.5691235901 -0.2598557930

S₀ energy / H -387.92443007312096

S₀ CI eigenvector 0.98724719543351 X36 X37 X38
-0.09231252203294 X36 X37 X39
-0.07473813237284 X37 X38 X39
-0.05810477880187 A36 X37 B38 X39
-0.05810477880187 B36 X37 A38 X39
0.03731851511057 X36 X37 A38 B39
0.03731851511057 X36 X37 B38 A39
-0.03662211345440 X36 X38 X39

S₁ energy / H -387.73435296924430

S₁ CI eigenvector -0.68776779599788 X36 X37 A38 B39
-0.68776779599788 X36 X37 B38 A39
0.12157726426136 A36 X37 X38 B39
0.12157726426136 B36 X37 X38 A39
0.09033090811472 X36 A37 B38 X39
0.09033090811472 X36 B37 A38 X39
0.05115726381170 X36 X37 X38
0.04896846654400 X36 X37 X39
-0.03442345199243 X37 X38 X39
-0.02903790866638 X36 A37 X38 B39

-0.02903790866638 X36 B37 X38 A39

eq-G+ S₀ Minimum (FC)

Cartesian coordinates / 26

Å

C	0.6960482445	-0.0870689034	0.1032427960
C	2.1626863025	-0.0576844258	-0.3832934109
C	-0.0884986580	1.1743503570	-0.2878428753
C	-0.0793547894	-1.3184258211	-0.3060929493
C	3.0166369418	-1.1085996037	0.3367219916
C	2.3167036572	-0.1977258456	-1.9026816995
C	-1.5530235132	1.0607302408	0.0506945782
C	-2.1888588477	-0.1141951421	0.0128325073
C	-1.4302457422	-1.3135032371	-0.3048362342
C	-3.6681042849	-0.2510727812	0.2682471986
H	0.7336829485	-0.0940102295	1.1955738903
H	2.5576055164	0.9177123264	-0.1028197183
H	0.0016911040	1.3541740970	-1.3593550705
H	0.3463757605	2.0390329813	0.2046486454
H	0.4495607089	-2.2299324216	-0.5185427318
H	2.7126398569	-2.1199528478	0.0833499680
H	4.0620250710	-1.0068359534	0.0609856035
H	2.9468010749	-1.0026704737	1.4151857457
H	1.9456648592	-1.1559234419	-2.2535025973
H	3.3639117843	-0.1292760459	-2.1822904325
H	1.7855179837	0.5777640602	-2.4427714802
H	-2.0947893591	1.9657719398	0.2677627609
H	-1.9718511037	-2.2187961190	-0.5217577433
H	-4.1243692097	0.7083293507	0.4818543027
H	-3.8594285947	-0.9124520087	1.1092605924
H	-4.1710277119	-0.6787400518	-0.5955736373

S_0 energy / H	-387.96128271615066
S_0 CI eigenvector	-0.97490610199104 X36 X37 X38
	0.11644922646756 X36 X37 X39
	-0.09740199834209 X36 X37 A38 B39
	-0.09740199834209 X36 X37 B38 A39
	0.08649470651096 X36 X38 X39
	-0.05806762497663 X36 A37 B38 X39
	-0.05806762497663 X36 B37 A38 X39
	-0.03149315218857 A36 X37 B38 X39
	-0.03149315218857 B36 X37 A38 X39
S_1 energy / H	-387.77296474415903
S_1 CI eigenvector	-0.66612638392567 X36 X37 A38 B39
	-0.66612638392567 X36 X37 B38 A39
	-0.16489117153764 X36 A37 X38 B39
	-0.16489117153764 X36 B37 X38 A39
	0.14235848364915 X36 X37 X39
	0.13452794941286 X36 X37 X38
	-0.09922599578473 X36 X38 X39
	0.04801419686799 X36 A37 B38 X39
	0.04801419686799 X36 B37 A38 X39
	-0.03528431505315 A36 X37 B38 X39
	-0.03528431505315 B36 X37 A38 X39
	-0.03316164040981 A36 X37 X38 B39
	-0.03316164040981 B36 X37 X38 A39

eq-G+ S_1/S_0 MECI-1 (Closed)

Cartesian coordinates /	C	0.7583159085	-0.1006263508	0.4949642215
Å	C	1.9487010256	-0.1456607667	-0.4810838568
	C	0.0362621951	1.2489130232	0.6182955523
	C	-0.4000957131	-0.9817307749	0.0920694465
	C	3.0843608934	0.7459294013	0.0315582008
	C	2.4451455340	-1.5766496329	-0.7138307309
	C	-1.4294795874	0.9137438898	0.7936023980
	C	-2.0935997272	0.1953150222	-0.2301624815
	C	-1.2901988639	-0.6302770664	-1.0040252554
	C	-3.5988551832	0.1826037232	-0.2949452518
	H	1.0962516366	-0.4122297405	1.4806115447
	H	1.6004122949	0.2458075544	-1.4326058947
	H	0.1762541409	1.8403927503	-0.2865916253
	H	0.4127924833	1.8305480182	1.4510988390
	H	-0.5440764187	-1.9126056505	0.6231471687
	H	3.4748676744	0.3721392274	0.9752809843
	H	3.9062817777	0.7730530190	-0.6774150585
	H	2.7549207141	1.7675084191	0.1912428782
	H	2.7521409499	-2.0476113045	0.2173166375
	H	3.3003600918	-1.5836978018	-1.3825883053
	H	1.6777242467	-2.1967451010	-1.1682206727
	H	-2.0081858679	1.4131702389	1.5502220112
	H	-1.7213068391	-1.3786644420	-1.6428089561
	H	-4.0031026839	1.1574858604	-0.0419692561
	H	-3.9948556205	-0.5392439088	0.4136463770
	H	-3.9349812458	-0.1001352588	-1.2851147592

So energy / H -387.80940292764240

So CI eigenvector -0.57871978062015 X36 X37 A38 B39

-0.57871978062015 X36 X37 B38 A39

-0.53617385164606 X36 X37 X38
0.11386776958470 X36 A37 B38 X39
0.11386776958470 X36 B37 A38 X39
-0.07835583232262 X36 A37 X38 B39
-0.07835583232262 X36 B37 X38 A39
0.05916993786748 X36 X38 X39
0.02260994333456 X37 X38 X39

S₁ energy / H -387.80940272617028

S₁ CI eigenvector 0.81952993002138 X36 X37 X38
-0.38119570043481 X36 X37 A38 B39
-0.38119570043481 X36 X37 B38 A39
-0.09724002381702 X36 X38 X39
0.08382713005827 X36 A37 X38 B39
0.08382713005827 X36 B37 X38 A39
0.07935555110863 X36 A37 B38 X39
0.07935555110863 X36 B37 A38 X39
-0.03504285474656 X37 X38 X39

eq-G+ S₁/S₀ MECI-2 (Closed)

Cartesian coordinates / 26
Å

C 0.8315692947 0.1936518889 0.2965853420
C 2.2488748655 0.0342300278 -0.3042589839
C -0.0646043360 1.2102494815 -0.4584503758
C 0.1274751178 -1.1172893598 0.5143741097
C 3.2624147346 -0.4860102298 0.7208815773
C 2.2727783115 -0.8253841500 -1.5744887382
C -1.5667438866 1.1714418026 -0.0693820186
C -2.0160138756 -0.1735338215 -0.0062272574

C	-1.2016932727	-1.2840778700	0.4753470157
C	-3.4129099395	-0.5031336533	-0.4366770891
H	0.9513282988	0.6005013115	1.3063549915
H	2.5607728611	1.0380565790	-0.5840049119
H	0.0094683597	1.0448079098	-1.5309233253
H	0.3310577267	2.2032964669	-0.2803775304
H	0.7345817273	-1.9740067991	0.7566192562
H	3.3340578954	0.1809041148	1.5743766335
H	2.9940964084	-1.4710820752	1.0945018293
H	4.2516965260	-0.5674029528	0.2809951803
H	2.0585066510	-1.8682404251	-1.3550400536
H	3.2539034249	-0.7913808219	-2.0374618744
H	1.5512536083	-0.4870484672	-2.3095571029
H	-1.3983297640	1.0683958322	1.0628601462
H	-1.6362366087	-2.2542421784	0.6455213089
H	-4.0928127451	-0.0525943141	0.2794246599
H	-3.6239923538	-1.5647047145	-0.5067538660
H	-3.5893352794	0.0039729897	-1.3780759565

So energy / H -387.80693665837327

So Cl eigenvector

-0.67990519954931	X36	X37	A38	B39
-0.67990519954931	X36	X37	B38	A39
-0.22899503431839	X36	X37	X38	
-0.08242271308404	A36	X37	B38	X39
-0.08242271308404	B36	X37	A38	X39
0.06073958417323	X36	A37	B38	X39
0.06073958417323	X36	B37	A38	X39
-0.02504941402394	X36	A37	X38	B39
-0.02504941402394	X36	B37	X38	A39
0.02176228949323	X37	X38	X39	

S₁ energy / H -387.80693659693350
S₁ CI eigenvector 0.95481877791196 X36 X37 X38
-0.16296049640291 X36 X37 A38 B39
-0.16296049640291 X36 X37 B38 A39
0.08705774046205 X36 A37 X38 B39
0.08705774046205 X36 B37 X38 A39
-0.08112785137459 X37 X38 X39
-0.06804658048944 X36 X38 X39
-0.05979856312741 A36 X37 X38 B39
-0.05979856312741 B36 X37 X38 A39
-0.02002049944278 A36 X37 B38 X39
-0.02002049944278 B36 X37 A38 X39

eq-G+ S₁/S₀ MECI-3 (Open)

Cartesian coordinates /
Å

26

C 0.8393340240 -0.1842733329 0.0702667985
C 2.3413296884 -0.1757239922 -0.1744777564
C -0.5134496424 1.2430574449 -0.9860143405
C -0.0193656647 -1.2093660117 -0.3304106005
C 3.1105786672 -0.1531246947 1.1549305307
C 2.8517825385 -1.3127529898 -1.0644544973
C -1.6916604615 1.1418784961 -0.2118601578
C -2.2114439674 -0.1278473010 0.0337061001
C -1.4289487822 -1.2635637487 -0.2356345117
C -3.6172771574 -0.2808463004 0.5510067190
H 0.5242766161 0.4342377115 0.8904969234
H 2.5902854585 0.7546639658 -0.6886958454

H	-0.4382334611	0.6920281665	-1.9045899679
H	0.0781506110	2.1413529522	-0.9482154056
H	0.4299577159	-2.0620520236	-0.8159763421
H	2.9413193639	-1.0671242670	1.7168988304
H	4.1797277991	-0.0522195241	0.9870992124
H	2.7947026510	0.6807948467	1.7749008549
H	2.7103178607	-2.2822464684	-0.5947365760
H	3.9141255320	-1.1935633428	-1.2520552820
H	2.3489934244	-1.3288369831	-2.0268865176
H	-2.0564048330	2.0022742172	0.3195550163
H	-1.9062515518	-2.2198941063	-0.3581808740
H	-4.2872514452	-0.4717969091	-0.2839040172
H	-3.9576001172	0.6240130942	1.0403949788
H	-3.7000937252	-1.1123041585	1.2408739903

S₀ energy / H -387.82076950452392

S₀ CI eigenvector -0.68673998548323 X36 X37 A38 B39
-0.68673998548323 X36 X37 B38 A39
0.19740638436937 X36 X37 X38
-0.08824148116916 X36 A37 B38 X39
-0.08824148116916 X36 B37 A38 X39

S₁ energy / H -387.82076928014169

S₁ CI eigenvector 0.95997457664482 X36 X37 X38
-0.14086373112353 X36 X38 X39
0.13894945635338 X36 X37 A38 B39
0.13894945635338 X36 X37 B38 A39
-0.08507873053137 X37 X38 X39
0.07221049275525 X36 X37 X39
-0.05062706457381 X36 A37 X38 B39

-0.05062706457381 X36 B37 X38 A39

0.02550730321154 X36 A37 B38 X39

0.02550730321154 X36 B37 A38 X39

eq-G+ cZc-EDOT Minimum

Cartesian coordinates / 26

Å

C	1.1069891144	-0.7071434348	0.1435385351
C	2.5967442049	-0.8780873330	-0.0446227292
C	-0.8185241000	2.1256866707	-0.5383397457
C	0.1373462659	-1.1905767785	-0.6249294365
C	3.2136466248	-1.5081232905	1.2136645063
C	2.9961560918	-1.6619931778	-1.2953199812
C	-1.4972466021	1.3737901447	0.3107580425
C	-2.0211864692	0.0157608187	0.0450907957
C	-1.3049009896	-1.0389914637	-0.4182374975
C	-3.5030402028	-0.1267083574	0.3145846343
H	0.8335645302	-0.1257240997	1.0085965066
H	3.0151856688	0.1248179686	-0.1377011611
H	-0.5372310951	1.7670350185	-1.5118288134
H	-0.5130731037	3.1242137821	-0.2797404200
H	0.4008133456	-1.8205237740	-1.4592070886
H	2.8462630536	-2.5202705978	1.3556113861
H	4.2961272098	-1.5491988451	1.1367846848
H	2.9652700445	-0.9374212340	2.1033944019
H	2.6298581219	-2.6836014882	-1.2549705960
H	4.0774024363	-1.7034303514	-1.3817157185
H	2.6087423078	-1.2007468222	-2.1976855500
H	-1.7781139413	1.8046241389	1.2615862602
H	-1.8710859596	-1.9242776642	-0.6627375201

	H	-3.7320318991	0.0763063957	1.3593564204
	H	-3.8538589751	-1.1266271484	0.0886782979
	H	-4.0815956827	0.5785109230	-0.2776982141
S_0 energy / H		-387.92458684230434		
S_0 CI eigenvector		0.98734756732215	X36 X37 X38	
		-0.09243563086125	X36 X37 X39	
		-0.07448575785208	X37 X38 X39	
		0.05767436211655	A36 X37 B38 X39	
		0.05767436211655	B36 X37 A38 X39	
		-0.03797202759569	X36 X38 X39	
		0.03607817069294	X36 X37 A38 B39	
		0.03607817069294	X36 X37 B38 A39	
S_1 energy / H		-387.73530515519013		
S_1 CI eigenvector		-0.68823877641986	X36 X37 A38 B39	
		-0.68823877641986	X36 X37 B38 A39	
		-0.11913239829799	A36 X37 X38 B39	
		-0.11913239829799	B36 X37 X38 A39	
		0.09078221553536	X36 A37 B38 X39	
		0.09078221553536	X36 B37 A38 X39	
		0.04950738469998	X36 X37 X38	
		0.04666626926509	X36 X37 X39	
		-0.03212382714577	X37 X38 X39	
		-0.03169745228226	X36 A37 X38 B39	
		-0.03169745228226	X36 B37 X38 A39	

Table S3.

Coordinates, Energies and CI Eigenvectors for S_0 And S_1 at Critical Points Along the Ring-Closed and Ring-Open Pathways of α PH. For the CI eigenvectors, XY indicates that the Y th molecular orbital is doubly occupied, and AYY/BYY indicate that the Y th molecular orbital is singly occupied with alpha or beta spin, respectively.

Supplementary Movies

**All movies were generated from the coordinate expectation value of a single AIMS trajectory basis function propagating first on S_1 and then spawned on S_0 using $\alpha(0.82)$ -SA2-CAS(6,4)-SCF/6-31G* and uPBE0/6-31G*, respectively.

1. (ax G+) aPH-CI1-cisL.mov
2. (ax T) aPH-CI1-cisL.mov
3. (eq G-) aPH-CI1-cisL.mov
4. (eq T) aPH-CI1-cisL.mov

These movies show the out-of-plane motion of C_4 in the ax/eq rotamers of aPH as the nuclear wavepacket propagates along the S_1 potential energy surface towards the CI-1 S_1/S_0 conical intersection (purple). The nuclear wavepacket moves away from the Frank-Condon region towards CI-1, where the C_4H bond pyramidalizes at approximately 90° to the molecular plane and the isopropyl group closely resembles its initial ax/eq configuration (see Fig. S8 for structural parameters). Upon relaxation to

vibrationally “hot” aPH (grey), a carbon-carbon bond is formed between C₇ and C₄, resulting in a relatively stable cis-Ladderane species.

5. (ax G-) aPH-CI3-ZZDOT.mov
6. (ax G+) aPH-CI3-ZZDOT.mov
7. (ax T) aPH-CI3-ZZDOT.mov
8. (eq G-) aPH-CI3-ZEDOT.mov
9. (eq G+) aPH-CI3-ZEDOT.mov
10. (eq T) aPH-CI3-ZEDOT.mov

These movies show the elongation of C₁-C₃ bond in the ax/eq rotamers of aPH as the nuclear wavepacket propagates along the S₁ surface towards CI-3 S₁/S₀ conical intersection (purple). The nuclear wavepacket moves away from the Frank-Condon region towards CI-3, where C₁-C₃ increases to ~2.30 Å and the isopropyl group closely resembles its initial ax G- configuration (see Fig. S8 for relative values). Upon relaxation, a vibrationally “hot” mixture of ZZDOT/ZEDOT structures are observed on the S₀ ground electronic state (grey). The Woodward-Hoffman expected ZZDOT/ZEDOT photoproducts are clearly formed in each trajectory.

11. (ax G+) aPH-CI1-aPH.mov
12. (ax T) aPH-CI1-aPH.mov
13. (eq G-) aPH-CI1-aPH.mov
14. (eq T) aPH-CI1-aPH.mov

These movies show the out-of-plane motion of C₄ in the ax/eq rotamers of aPH as the nuclear wavepacket propagates along the S₁ potential energy surface towards the CI-1 S₁/S₀ conical intersection (purple). The nuclear wavepacket moves away from the Frank-Condon region towards CI-1, where the C₄H bond pyramidalizes at approximately 90° to the molecular plane and the isopropyl group closely resembles its initial ax/eq configuration (see Fig. S8 for structural parameters). Upon relaxation, vibrationally “hot” aPH is observed on the S₀ ground electronic state (grey) where axial-to-equatorial isomerization (and vice-versa) is observed in both conformers.

15. (ax G+) aPH-CI2-aPH.mov
16. (ax G-) aPH-CI2-aPH.mov
17. (ax T) aPH-CI2-aPH.mov
18. (eq G+) aPH-CI2-aPH.mov
19. (eq G-) aPH-CI2-aPH.mov
20. (eq T) aPH-CI2-aPH.mov

These movies show the out-of-plane motion of C₇ in the ax/eq rotamers of aPH as the nuclear wavepacket propagates along the S₁ potential energy surface towards the CI-2 S₁/S₀ conical intersection (purple). The nuclear wavepacket moves away from the Frank-Condon region towards CI-2, where the C₇H bond is oriented at approximately 90° to the molecular plane and the isopropyl group closely resembles its initial ax/eq configuration (see Fig. S8 for structural parameters). Upon relaxation, a vibrationally “hot” aPH is observed on the S₀ ground electronic state (grey).

21. (ax G+) aPH-CI3-aPH.mov
22. (ax G-) aPH-CI3-aPH.mov
23. (ax T) aPH-CI3-aPH.mov
24. (eq G+) aPH-CI3-aPH.mov
25. (eq G-) aPH-CI3-aPH.mov
26. (eq T) aPH-CI3-aPH.mov

These movies show the elongation of C₁-C₃ bond in the ax/eq rotamers of aPH as the nuclear wavepacket propagates along the S₁ surface towards CI-3 S₁/S₀ conical intersection (purple). The nuclear wavepacket moves away from the Frank-Condon region towards CI-3, where C₁-C₃ increases to ~2.30 Å and the isopropyl group closely resembles its initial ax G- configuration (see Fig. S6 for relative values). Upon relaxation, a vibrationally “hot” aPH is observed on the S₀ ground electronic state (grey).